# Final report

## 1.1 Project details

| | |
|---|---|
| **Project title** | Maturing Solid Oxide Electrolyser Technology |
| **Project identification (program abbrev. and file)** | Maturing SOEC (64015-0523) |
| **Name of the programme which has funded the project** | EUDP |
| **Project managing company/institution (name and address)** | Haldor Topsoe A/S<br>Haldor Topsøes Allé 1<br>2800 Kgs. Lyngby |
| **Project partners** | Haldor Topsoe A/S (HTAS)<br>DTU Energy – Department of Energy Conversion and Storage (DTU)<br>Danish Solar Energy Ltd (Dansk Solenergi ApS) - DSOL |
| **CVR** (central business register) | 41853816 |
| **Date for submission** | 31/5-2019 |

## 1.2 Short description of project objective and results

### *1.2.1 English version*

The main objective of the project was to mature the solid oxide electrolysis cell (SOEC) technology to a level where competitive applications can grow from niche markets to significant segments of the specialty gas and off-grid power storage markets requiring extended storage time. Niche markets serve as stepping-stones for further maturing of the technology, however, challenges related to degradation, robustness and cost must be solved before upscaling to multi-MW SOEC-based systems can be realized.
Significant progress was made on improving degradation and robustness both on cell and stack level. The results will hopefully facilitate market penetration in certain niche markets for SOEC. HTAS is currently focusing on commercialization of their unique cost-competitive eCOs™ technology for converting $CO_2$ to CO, which is relevant for several different industries.

### *1.2.2 Danish version*

Hovedmålet med projektet var at modne faststof oxid elektrolyse celle (SOEC) teknologien til et niveau hvor konkurrencedygtige applikationer kan vokse fra niche markeder til betydelige dele af markederne inden for specialitets gas og afkoblet strøm-lagring, hvor langtids-lagring er påkrævet. Niche markeder benyttes som trædesten for at modne teknologien, dog må udfordringer relateret til degradering, robusthed og omkostninger overkommes før en opskalering til multi-MW SOEC-baserede systemer kan blive en realitet.
Betydelige fremskridt blev opnået mht. forbedring af degradering og robusthed på både celle og stak niveau. Resultaterne vil forhåbentlig muliggøre markedsindtrængning for SOEC teknologien inden for visse niche markeder. HTAS fokuserer på nuværende tidspunkt på kommercialisering af deres unikke og prismæssigt konkurrence-dygtige eCOs™ teknologi for omdannelse af $CO_2$ til CO, hvilket er relevant for flere forskellige industrier.

## 1.3 Executive summary

Significant progress was made during the project on improving degradation and robustness of the solid oxide electrolysis cell (SOEC) technology, both on cell, stack, and system

relevant level. The understanding of SOEC specific degradation mechanisms is key to increasing the lifetime of the technology and bringing down costs. The Technical University of Denmark (DTU) furthered the understanding of several important degradation mechanisms, including Ni-migration, carbon deposition, and requirements on gas purity. Improved knowledge will allow future innovative solutions to mitigate or minimize the specific degradation mechanism.
Enhanced multi-physics modelling tools were developed for faster evaluation of design modifications and better understanding of thermo-mechanical stresses inside a stack. The advanced simulation tools were successfully used for finding safe operating protocols for various electrolysis modes. The improved modelling tools developed in the project will be used by Haldor Topsoe for future stack modifications and to conduct virtual prototyping, which will save development time and speed up the time from idea to product.

Highly advanced stack testing was carried out at DTU Energy. Electrochemical impedance spectroscopy (EIS) was measured during reversible operation of Haldor Topsoe's commercial stack, pressurized operation up to 18.7 bar was carried out on a small SOFCMAN stack, and internal methanation was shown. Pressurized operation of a Haldor Topsoe commercial stack was likewise attempted, but given the size and complexity, additional work on the equipment is required. This will be pursued in future projects.

More than one year operation in $CO_2$ electrolysis was shown in a system level test (SOEC Core), and improved SOEC stacks at the end of the project showed potential for lifetimes >2 years (tests still ongoing). Many of the learnings from this project have or will be implemented in coming upgrades to Topsoe's stack platform and will be further investigated in future collaborative projects. The results will hopefully facilitate market penetration in certain niche markets for SOEC. HTAS is currently focusing on commercialization of their unique cost-competitive eCOs™ technology for converting $CO_2$ to CO, which is relevant for several different industries.

It has been confirmed that various niche markets can serve as stepping-stones for maturing the SOEC technology, in order to reach larger markets in the future. By accomplishing most of the main objectives in the project we will get closer to commercialization of the technology. Recent commercial activities related to Haldor Topsoe's eCOs™ technology is a confirmation that the SOEC technology has matured and can solve current challenges in the industry at a cost-competitive price, once appropriate niche markets are targeted.

Danish Solar Energy (DSOL) has successfully developed power electronics (SMART controller) in the project, which they aim to use in various energy storage solutions, e.g. battery storage solutions. With the gained knowledge from this project, DSOL are now able to predict several key factors optimizing the storage solutions, which will give them an advantage to supply custom-made solutions and hereby optimize and reduce the system cost and potentially extend their revenue.

### 1.4 Project objectives

The solid oxide electrolysis cell (SOEC) technology has developed significantly over the last decade, but there are still challenges related to degradation, robustness and cost that must improve before upscaling SOEC-based electrolysis plants to multi-MW scale can be realized. Certain niche markets can serve as stepping-stones for maturing the technology. In order to realize the overall objective, the project focused on three key objectives:

1. Mitigate the main degradation and robustness challenges on cell and stack level.
2. Demonstrate pressurized reversible operation. Such operation can reduce system cost and improve the conversion efficiency.
3. Approach niche markets to mature the SOEC technology for large-scale energy storage and grid-balancing market requirements.

The project was implemented by having 5 different work packages (WP) focusing on different critical topics.

WP1 focused on improving reliability and lifetime of the state-of-the-art (SoA) cells to withstand known degradation mechanisms and by investigating for unknown long-term mechanisms. This was achieved by testing cells >10kh, and investigating dynamic and harsh operating conditions. A lot of focus in the project has been on furthering the understanding of one of the most critical degradation mechanisms on cell level, Ni-migration. A dedicated workshop was held with experts in the field of Ni agglomeration and sintering (including catalysis experts from HTAS). New ideas were suggested for mitigating the Ni-migration issue and it was deemed more essential to understand these new solutions on cell level before trying to implement them in full-sized stack tests. A novel Ni-free cell concept was investigated in the project. The new cell design is looking promising and the concept is under consideration for a patent application. Therefore, no results will be presented in this report. More research will be needed to show proof-of-concept and will hopefully be investigated in coming projects. Cell tests in $CO_2$ electrolysis surprisingly revealed that minor impurities (on ppb level) significantly reduces the lifetime of the cells. This knowledge is very important when designing systems for $CO_2$ electrolysis.

In WP2 the main objectives were to determine critical stack lifetime limiting phenomena as well as stack end-of-life criteria and to develop stacks to mitigate these issues. Electrochemical impedance spectroscopy was used on stack level to detect conditions and locations for critical degradation. Another focus was long-term testing of stacks (SOEC Core with 2 stacks) and to demonstrate >1 year operation, which was successfully achieved. By project end, improved stacks were developed and tested based on input from other WPs, with the aim of showing the potential for longer (>2 years) stack lifetime.

WP3 focused on improving advanced multi-physical models, which were used to optimize specifics in the cell and stack designs. The models were furthermore enhanced to describe mechanical failures and to specify a window for safe operation conditions. The safe operation window was validated on real stacks in WP2. To optimize local geometric features in the stack a 2D model describing this was developed. The output from the model was eventually used for stack improvements.

The most challenging tasks, with highest risks, were performed in WP4. Here it was attempted to demonstrate efficient electricity storage by operating SOEC stacks reversibly and pressurized. Reversible operation of stacks was demonstrated at atmospheric pressure. However, technical difficulties with the high pressure setup at DTU (related to testing equipment and resources) resulted in unsuccessful high-pressure testing of technologically relevant stacks from HTAS. Nevertheless, proof-of-concept on a simpler stack platform was conducted, where it was shown that internal methanation is possible during co-electrolysis (electrolysis of steam and $CO_2$) at elevated pressure. Further work is needed to verify this on state-of-the-art stacks from HTAS.

Finally, WP5 focused on analyzing market opportunities and demonstration of system components. One objective was to conduct a market study for small-scale off-grid power systems requiring extended storage time. This work was done by Danish Solar Energy (DSOL). Based on knowledge from combined solar cells and battery solutions, design and development of optimized power electronics for electrolysis-based off grid power storage systems was conducted. Various low cost small-scale hydrogen storage solutions conceptually evaluated and a potential proof-of-concept was schematically demonstrated. In WP5 HTAS also evaluated their first commercial demonstration unit for on-site on-demand production of CO from $CO_2$ (eCOs™). The unit was started at Gas Innovations in La Porte, Texas, USA during Q1 2016 and has been successfully operated with increasing interest from the market during the project. HTAS has focused on increasing the awareness of the eCOs™ technology to various markets around the globe since the start of the first unit. The conclusion is that HTAS need to maintain a stepping-stone approach in order to reach the future larger markets. HTAS must bridge the gap between the current eCOs™ solution and a technical solution in the future (beyond 2030), where the vision and ambition is that SOEC will be the cheapest and preferred $H_2$ and CO production method, with large capacity, low cost and large scale production.

In the project there were in total 19 milestones. Out of these 19 milestones, five key milestones and two "commercial milestones" (CM) were highlighted as important in order to accomplish the overall objectives of the project:

- **M1.1** – Demonstrate SOEC single cell lifetime exceeding 10 kh – *Milestone fulfilled*
- **M2.4** – More than one year operation of a stack demonstrated – *Milestone fulfilled*
- **M2.5** – Optimized cells with improved lifetime tested in a stack with improved designs, show potential for longer (>2 year) lifetime – *Milestone fulfilled*
- **M4.3** – Electricity storage based on dynamic pressurized reversible operation of SOCs demonstrated – *Milestone not fulfilled*
- **M5.2** – Small-scale low-cost hydrogen storage concept demonstrated – *Milestone partially fulfilled*
- **CM1** – Report on market analysis of off-grid power systems requiring extended storage time - *Milestone fulfilled*
- **CM2** – Analysis of field testing data from small-scale syngas production unit – how to reach the next market - *Milestone fulfilled*

In total 15 out of 19 milestones were fulfilled in the project, two partially fulfilled, and two milestones were unfortunately not accomplished. With the results obtained in the project we are confident that the SOEC technology has matured significantly and will facilitate market penetration in certain niche markets for SOEC in the coming few years (1-3 years).

## 1.5 Project results and dissemination of results

### *1.5.1 Overview and milestones*

The project was structured into five technical work packages (WPs), which were further divided into work tasks as listed in the overview below:

- WP1: Improving reliability and lifetimes of cells
  - WP1.1: Demonstrating years of reliable operation of SOEC cells
  - WP1.2: Critical lifetime limiting conditions and mechanisms
  - WP1.3: Cells with improved reliability and longer lifetime
- WP2: Mitigating critical degradation mechanisms in stacks
  - WP2.1: Performance mapping of stacks during SOEC operation using EIS
  - WP2.2: Long-term testing and end-of-life criteria on stack level
  - WP2.3: Improved stack design and operation for enhanced reliability and lifetime
- WP3: Optimized cells and stacks by advanced modelling
  - WP3.1: Enhancement of 3D multi-physics model to simulate mechanical failures
  - WP3.2: Development and implementation of 2D sub-model
  - WP3.3: Identification and measurement of parameters for modelling
  - WP3.4: Predicting a window for safe stack operation
- WP4: Development of reversible and pressurized operation of SOECs
  - WP4.1: Reversible operation – possibilities and limitations
  - WP4.2: Pressurized SOEC operation
  - WP4.3: Pressurized and reversible systems and electricity storage demonstration
- WP5: Analyzing market opportunities and demonstration of system components
  - WP5.1: Analyses of off-grid power systems with enhanced storage time
  - WP5.2: Demonstration of power electronics systems optimized for SOEC/SOFC-based off-grid power storage systems
  - WP5.3: Demonstration of small-scale low-cost hydrogen storage
  - WP5.4: Analyses of field testing data from small-scale syngas production unit

In Table 1 are the milestones that were set up in the project plan and their overall status at the completion of the project.

***Table 1.*** *Overview of project milestones and their status at project end.*

| Milestone | Description | Status |
|---|---|---|
| **M1.1 (KEY)** | Demonstrate SOEC single cell lifetime exceeding 10 kh at realistic stack operating conditions. (DTU) | **Fulfilled** |
| **M1.2** | Magnitude of contact resistances between cell and metallic interconnects evaluated on cell testing level. (DTU) | **Fulfilled** |
| **M1.3** | Cell test with dynamic operation schemes conducted and analysis of the lifetime limiting mechanisms achieved. (DTU) | **Fulfilled** |
| **M1.4** | Cells with improved lifetime developed, produced, and delivered to WP2 for stack testing. (DTU) | Not fulfilled |
| **M2.1** | Extended stack testing protocol with impedance spectroscopy developed and tested on a large (>40 cell) stack. (DTU) | **Fulfilled** |
| **M2.2** | Report on End-of-Life criteria (DTU) | **Fulfilled** |
| **M2.3** | At least 3 stacks tested for at least 1000 hours (input and validation of 3D models). (HTAS) | **Fulfilled** |
| **M2.4 (KEY)** | More than one year operation of a stack for syngas production demonstrated. (HTAS) | **Fulfilled** |
| **M2.5 (KEY)** | Optimized cells with improved lifetime tested in stack with improved design – show potential for longer (2 year) lifetime. (HTAS) | **Fulfilled** |
| **M3.1** | Model for homogenization of the creep and contact demonstrated and made available for investigations. (DTU) | **Fulfilled** |
| **M3.2** | 2D unit cell model finalized. (HTAS) | **Fulfilled** |
| **M3.3** | Window for safe stack operation modelled and analysed. (HTAS) | **Fulfilled** |
| **M4.1** | Possibilities and limitations identified for extended SOEC stack lifetime using reversible operation. (DTU) | **Fulfilled** |
| **M4.2** | Technologically relevant HTAS stacks tested at elevated pressure. (DTU) | Partially fulfilled |
| **M4.3 (KEY)** | Electricity storage based on dynamic pressurized reversible operation of SOCs demonstrated. (DTU) | Not fulfilled |
| **M5.1** | Demonstration of power electronics systems optimized for SOEC/SOFC-based off grid power storage systems. (DSOL) | **Fulfilled** |
| **M5.2 (KEY)** | Small-scale low-cost hydrogen storage concept demonstrated. (DSOL) | Partially fulfilled |
| | | |
| **CM1** | Report on market analysis of off-grid power systems requiring extended storage time. (DSOL) | **Fulfilled** |
| **CM2** | Analyses of field testing data from small-scale syngas production unit – how to reach the next market. (HTAS) | **Fulfilled** |

### *1.5.2 WP1: Improving reliability and lifetimes of cells*

The three main objectives of WP1 was demonstrating years of lifetime for SOECs on single-cell level (WP1.1), investigate and understand any critical lifetime limiting degradation mechanisms (WP1.2), and lastly, developing the cells to increase the potential lifetime (WP1.3).

### 1.5.2.1 WP1.1: Demonstrating years of reliable operation of SOEC Cells

***M1.1: Demonstrate SOEC single cell lifetime exceeding 10 kh at realistic stack operating conditions (KEY)***

**Cell specifications**

The cell used for the 10 kh test was a fuel electrode supported full SOEC produced at DTU Energy. The cell is a Ni/YSZ supported Ni/YSZ-YSZ-$CGO_{barrier}$-LSC/CGO based cell [1]. The cells consisted of a 12-16 μm thick Ni/YSZ fuel electrode with a ~300 μm thick Ni/YSZ support layer, a ~10 μm thick YSZ electrolyte, a 6-7 μm thick CGO barrier layer and a ~30 μm thick LSC/CGO oxygen electrode [2]. For the production of the support layer, active fuel electrode, electrolyte and CGO barrier layer successive tape casting i.e. a multilayer tape casting (MTC) process and lamination process was applied [1]. These four MTC layers of the tapes were co-sintered at 1315 °C [3] and cut into 53x53 $mm^2$ cells. The oxygen electrode (40x40 $mm^2$) was applied by screen-printing and sintered at 930 °C. Afterwards, a LSM contact layer was applied by screen-printing. The set-up for single cell testing was illustrated and described in detail previously [4,5].

**Test conditions**

Test conditions for single cell test for WP1.1 were selected based on input from stack modelling results received from HTAS. The test conditions for the 10 kh galvanostatic single cell test were set to mimic realistic stack outlet operating conditions; at an average temperature of 695 °C, inlet gas mixture of 84% $H_2O$ and 16% $H_2$ with a steam conversion of 11% and leading air to the oxygen electrode. The current density was kept at -0.3 $A/cm^2$ throughout the test and impedance spectra were recorded regularly during electrolysis.

**Cell test results**

Figure 1 shows the development of cell voltage, ohmic resistance ($R_S$) and polarization resistance ($R_P$) over the 10 kh single cell steam electrolysis test. The cell voltage was 1087 mV at start of electrolysis testing increasing to 1212 mv after 5 kh of testing and ending at 1267 mV at end of test which gives a voltage degradation rate of 18 mV/kh corresponding to 1.66%/kh for the entire 10 kh test. Considering only the last 5 kh of testing the voltage degradation rate was only 11 mV/kh corresponding to 0.90 %/kh and this exhibited a very linear degradation behavior. Notice, that the cell voltage is still below thermoneutral potential after 10 kh of electrolysis operation.

Only a very limited and linear increase in $R_S$ is observed over the 10 kh of galvanostatic steam electrolysis testing. For the degradation related to increase in $R_P$, the test can roughly be divided int o two parts. First an "initial" non-linear and dominating $R_P$ degradation within the first 1-2 kh. Hereafter, a less pronounced and more or less linear $R_P$ increase can be observed for the 10 kh test. The "initial" degradation is dominated by an increase in the resistance originating from the charge transfer reaction giving rise to a polarization resistance contribution with a characteristic frequency around 1-5 kh. Analysing the development of the polarization resistance over the last 5 kh of the test it is clearly in the very low frequency (below 1 Hz) part of the impedance spectrum that the impedance increase while being surprisingly stable at higher frequencies.

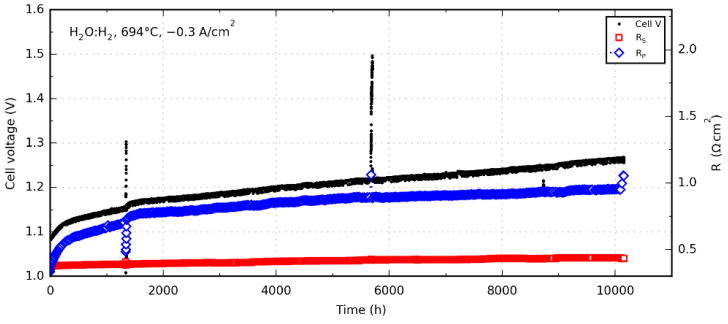


***Figure 1.*** *Development of cell voltage, ohmic resistance ($R_s$) and polarization resistance ($R_P$) over 10 kh galvanostatic steam electrolysis test.*

**Post-mortem microscopy**

During the final fingerprint (characterization of the cell), cell voltage and $pO_2$-out measurements indicated breakage or significantly increased leakage in the cell. Besides visual inspection (green colored parts) during dismounting, post-mortem SEM confirmed oxidation of parts of the middle and outlet of the cell and cracks in the electrolyte; see Figure 2A). Figure 2B) shows a low voltage inlens SEM micrograph (in which the bright particles are Ni constituting a connected network) on the gas inlet part of the cell for a part of the cell that was at OCV during the entire test, while the micrograph in Figure 2C) is from part of the cell that experienced a current load of at least -0.3 A/cm$^2$. There are only small differences between these two micrographs; especially when compared to the two micrographs given in the article by Mogensen et al. [6]; for a similar cell tested with an inlet gas of 90% $H_2O$ in $H_2$, at 800 °C, but at a significantly higher current load of -1.0 A/cm$^2$. The finding in Figure 2B) and C) fits well with the analysis of impedance data during test. Analysis of the impedance spectra after 2 kh suggest that the electrochemical part of the fuel electrode resistance was around 0.41 Ωcm$^2$ corresponding to 129 mV overpotential and even after 3 kh was the electrochemical contribution to the fuel electrode overpotential below 155 mV. In the work by Hauch et al. [7] it was shown that a fuel electrode overpotential of 155 mV was enough to avoid extended and detrimental Ni depletion over 2 kh while a fuel electrode overpotential of ~300 mV was shown to lead to severe Ni depletion already after 1 kh.

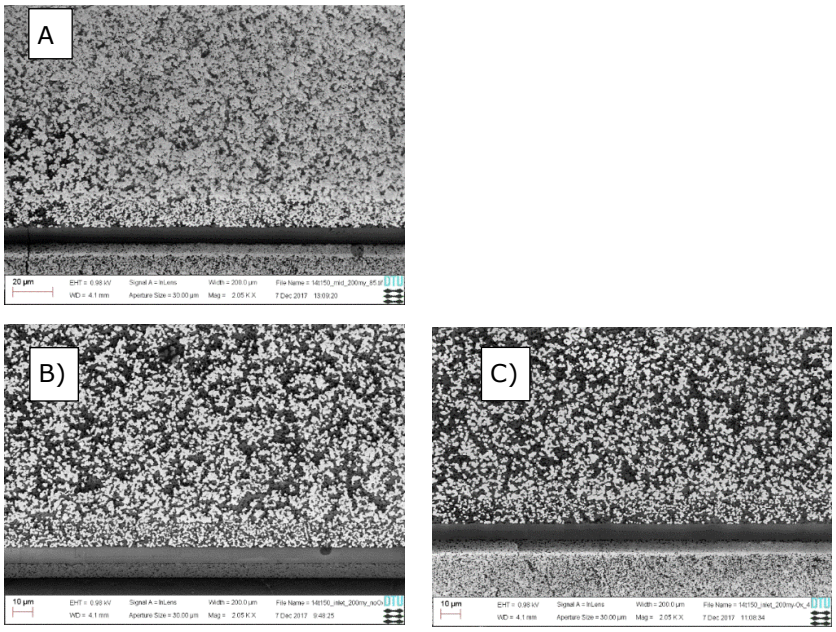


***Figure 2.*** *Low-voltage inlens SEM images of the 10 kh tested single SOEC with the fuel electrode support layer in top part of each micrograph. A) Partly oxidized middle part of the cell, B) Gas inlet part of the cell (at OCV, no oxygen electrode at boarder of the cell) and C) Gas inlet part of the cell, which experienced a current density of at least -0.3 A/cm$^2$.*

**Conclusions**

Milestone 1.1 was accomplished. In the project we demonstrated SOEC single cell lifetime exceeding 10 kh at realistic stack operating conditions; ie. at 695 °C, inlet gas mixture of 84% $H_2O$ and 16% $H_2$ with a steam conversion of 11% and air to the oxygen electrode. The current density was kept at -0.3 A/cm$^2$ throughout the test. In total, the cell voltage increased from 1087 mV to 1267 mV after 10 kh of electrolysis operation. Over the last approximately 8 kh of test the cell voltage degradation was linear and corresponding to a voltage degradation of only 0.9 %/kh. Only very limited Ni depletion was observed in the inlet part of the cell via SEM imaging.

### 1.5.2.2 WP1.2: Critical lifetime limiting conditions and mechanisms

One of the major lifetime limiting mechanisms were known from previous projects to be the contact resistance between cells and the metallic interconnects. This issue was investigated in greater detail as described below.

***M1.2: Magnitude of contact resistances between cell and metallic interconnects evaluated on cell testing level***

**Abstract**

This section presents the results from two single repeating unit (SRU) tests conducted in the project. The purpose of the two tests is to study a) the influence of mechanical weight load on the SRU performance, and b) the influence of the gas channel configuration on the fuel utilization. The first test revealed that it was possible to completely remove the mechanical weight load without affecting the interfacial contacting. Even after a full thermal cycle without weight load, the SRU performance was intact. The second test had flat interconnects with no gas channels. Instead the gas passed through foams placed adjacent to the electrodes. This was observed to improve the fuel utilization. Gas channels infer a local variation of the gas concentration. The improvement is most likely related to the removal of this local variation.

**Introduction**

The two SRU tests were performed with multilayer tape casted Ni-YSZ electrode supported SOC cells with a CGO inter-diffusion barrier layer, an LSC-CGO oxygen electrode and an LSC contact layer. The interconnector and current collector plates were made of Crofer 22 APU. CuMn metal foam and Ni foam were used as contact material at the oxygen electrode and fuel electrode. The oxygen electrode side of the interconnector plate was coated $MnCo_2O_4$. No coating was used on the fuel electrode side of the interconnector plate.
The test schedule and operation conditions are outlined in Figure 3.

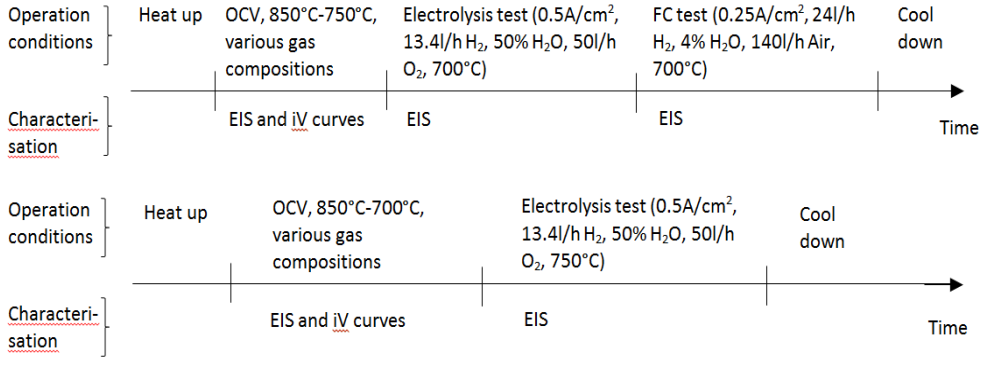


***Figure 3.*** *Operation conditions for SRU test 1 (top) and 2 (bottom).*

**Results and discussion**

For both test 1 and 2, after a short standard fingerprint, a constant current test was started under -0.5 A/cm$^2$ at 750 °C with 10% $H_2$ + 90% $H_2O$ supplied to the fuel electrode compartment and $O_2$ to the oxygen electrode compartment, the steam conversion was 28%. For test 1, during the constant current characterization, the mechanical weight load was decreased from 50 Kg at the start up to 0 kg at the end of the test. An additional thermal cycle performance characterization was performed before completely shutting down the test. A second SRU test was performed to compare the performance with the first test. The first test was performed with strip rib ICs and the second one was performed with flat ICs, where the electrode gasses diffused through the foams.
The operation history for Test 1 can be seen from Figure 4 (Left). As mentioned above, mechanical weight load was reduced during the constant current operation to check the influence of weight load on the SRU performance. The SRU voltage (measured between the

two ICs) and the cell voltage (measured between the two contact foams) as well as weight load evolution with time are plotted in Figure 4 (Right).

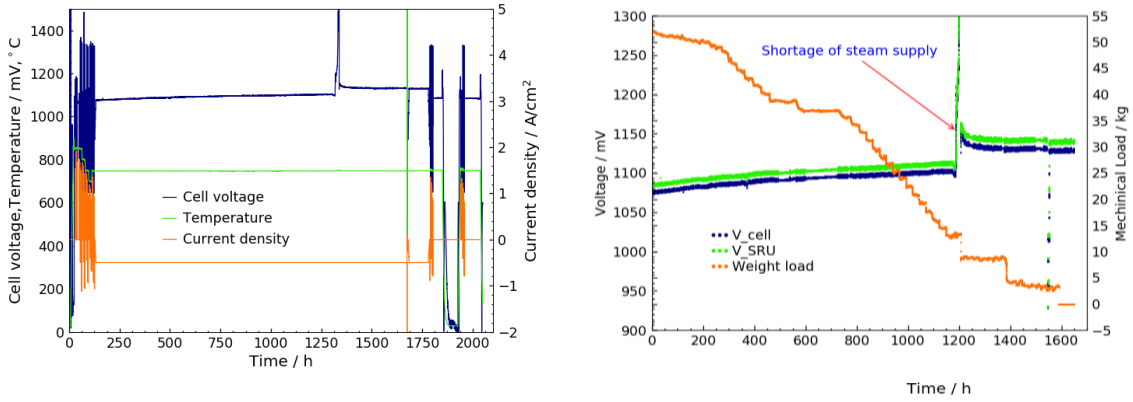


***Figure 4.*** *Left) Operation history of the SRU test 1. Right) SRU voltage, cell voltage and weight load as function of operation time during the constant current operation at -0.5 A/cm².*

It can be seen from Figure 4 (Right) that changing of mechanical weight load did not affect the SRU's performance as there was no noticeable correlation between voltages evolution and weight load changes. The sharp increase of voltages at around 1200 hours operation was due to the short period shortage of steam supply, and the cell was operated at close to 100% steam utilization for a short period and as a result the voltages increased around 30 mV even after the reset of steam supply. However, no accelerated degradation was observed afterwards in the last 500 hours operation. The impedance spectra measured during the constant current/weight load changing operation confirmed the aforementioned observation.

Figure 5 presents the time evolution of the serial resistance Rs, polarization resistance Rp and the total area specific resistance ASR that extracted from the impedance spectra. It can be seen that only minor changing of Rs during the constant current operation/weight load changing, and the Rs jump at around 1200 hours may be attributed to the shortage of steam supply. This indicated that during the decreasing of weight load, no measureable contact loss was introduced.

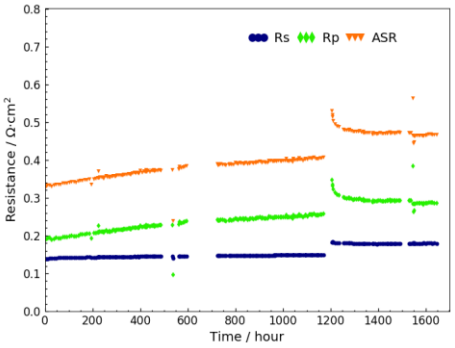


***Figure 5.*** *Rs, Rp and ASR as function of operation time.*

Figure 6 presents the impedance spectra and the corresponding DRT analysis of the spectra. It can be seen that during the test, the low frequency process, conversion arc was constant, indicating that no gas bypass arose during the operation. Degradation can be seen from the high frequency part with summit frequency shifted from 10 kHz to around 2 kHz which can be attributed to the fuel electrode degradation. Relative large change both on the fuel electrode and oxygen electrode can be seen after the shortage of steam supply, which may cause partial damage of the cell, even though no accelerated degradation was seen afterwards, the cell voltage increased around 30 mV.

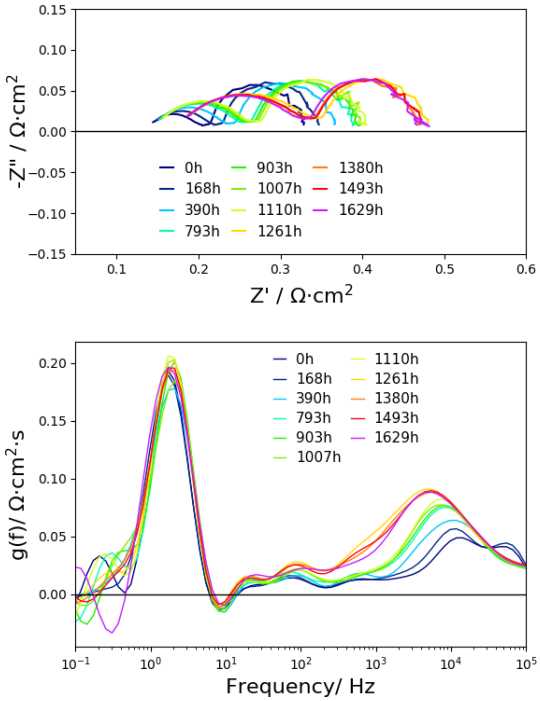


***Figure 6.*** *Impedance spectra and DRT analysis of the impedance recorded during the constant current operation.*

A thermal cycle was performed almost without mechanical weight load. (the residual weight load of the top part of the SRU test house remained during the test) before the test was shut down. A fingerprint was carried out to check the performance loss. The result is presented in Figure 7 and Figure 8. It can be seen from both the IV and the EIS characterization that almost no degradation occurred during the thermal cycle.

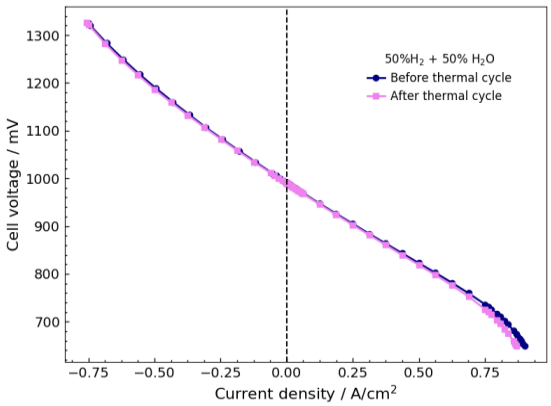


***Figure 7.*** *IV characterization before and after the thermal cycle at 750 ℃ with 50% $H_2$ + 50% $H_2O$ supplied to the fuel electrode and $O_2$ supplied to the oxygen electrode.*

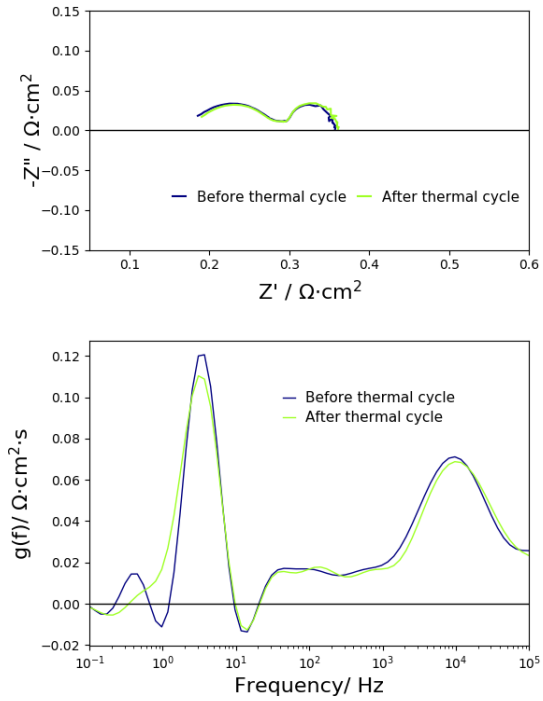


***Figure 8.*** *EIS characterization before and after the thermal cycle at 750 ℃ with 50% $H_2$ + 50% $H_2O$ supplied to the fuel electrode and $O_2$ supplied to the oxygen electrode.*

The test results of the first SRU test shows that, after the SRU has been heat treated at high temperature and high mechanical weight load, the contact can be maintained with almost no mechanical compression, and it can also cope with the potential stress introduced during the fingerprint and thermal cycle.

The second SRU test was performed to compare the performance with the aforementioned test 1. The main difference between the two tests relates to the setup. The first test was performed with strip rib ICs and the second one was performed with flat ICs. The iV and EIS characterization results (Figure 9 and Figure 10) were conducted at 750 °C. It is seen from iV that the first test has better performance at low current density but also show an early reactant starvation at high current. The EIS showed that the two tests have similar polarization resistance, but the second test with flat IC has almost twice higher Rs compared with the first test. By comparing the two tests, it is can tentatively be concluded that flat ICs with foams provide more uniform gas distribution than corrugated ICs (i.e. less gas bypass in the gas channels), although contact improvement are required.

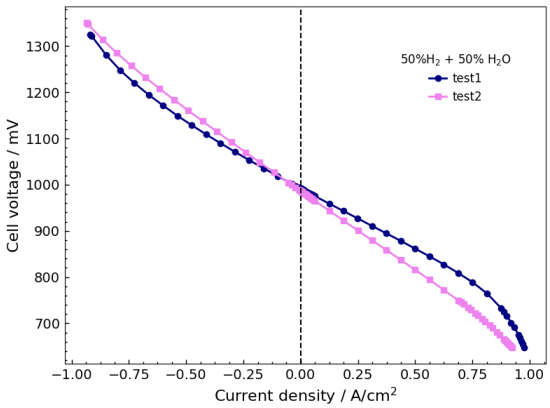


***Figure 9.*** *IV characterization comparison at 750 ℃ with 50% $H_2$ + 50% $H_2O$ supplied to the fuel electrode and $O_2$ supplied to the oxygen electrode.*

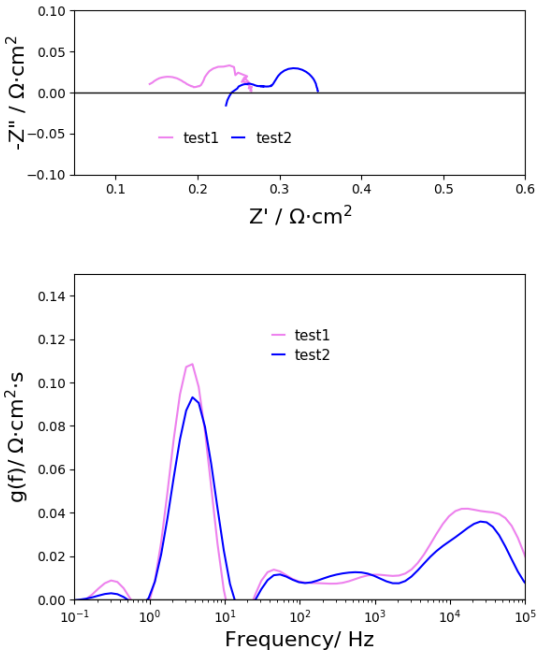


***Figure 10.*** *EIS characterization comparison at 750 ℃ with 50% $H_2$ + 50% $H_2O$ supplied to the fuel electrode and $O_2$ supplied to the oxygen electrode.*

**Conclusion**

From the SRU tests it is concluded that after formation of glass seals, the seals are strong enough to withstand load-free thermal cycles, and dynamic operation. Further, from comparing iV curves and impedance data from two different SRU configurations, it is observed that improved fuel flow uniformity and decreased gas concentration overvoltage (and related constraints on e.g. $CO_2$ electrolysis and maximum CO concentration in the SOEC outlet gas) can be obtained with flat ICs and current collector foams.

### 1.5.2.3 WP1.3: Cells with improved reliability and longer lifetime

During the project it became clear that M1.3 should be focused on a specific lifetime limiting degradation mechanism, namely poisoning of the fuel electrode by gas impurities. A study was undertaken to investigate to what extent gas cleaning is required during $CO_2$ electrolysis, where poisoning has previously been shown to have more dramatic effect on the lifetime [8,9].

***M1.3: Cell test with dynamic operation schemes conducted and analysis of the lifetime limiting mechanisms achieved.***

**Abstract**

Cell testing with different gas qualities at stack relevant conditions was carried out and the results were compared with similar operation in steam electrolysis. While long-term durability can be obtained for $H_2O/H_2$ test conditions (test A), detrimental degradation occurs for the $CO_2$/CO tested cells. We demonstrate that different cells show similar high degradation rates when tested under conditions where part of the produced CO is recycled and re-used as feed along with fresh $CO_2$, which strongly suggests that it is not impurities in the CO, but impurities in the $CO_2$ that initiates the observed degradation. The degradation can exclusively be attributed to an increase in polarization resistance from the Ni/YSZ electrodes. Various post-mortem analyses of the tested cells reveal carbon deposits in the fuel electrodes, despite operating far from carbon inducing conditions. This study therefore includes attempts at specifying the threshold for $CO_2$ gas quality to avoid overpotential-driven carbon formation and thereby mitigating the detrimental fuel electrode degradation.

**Cell specifications**

Ni/YSZ supported Ni/YSZ-YSZ-$CGO_{barrier}$-LSC/CGO based cells similar to previous sections were produced at DTU Energy. The cells consisted of a 10-15 μm thick Ni/YSZ fuel electrode with a ~300 μm thick Ni/YSZ support layer, a ~10 μm thick YSZ electrolyte, a 6-7 μm thick CGO barrier layer and a ~30 μm thick LSC/CGO oxygen electrode. 8YSZ was used for the electrolyte and the active fuel electrode layers. 3YSZ was used for the support layer [7,10]. Cells with volume ratios of Ni/YSZ ratio 50/50 and 40/60 volume percent in the fuel electrode were produced for this study [11]. For Test D, a cell produced at HTAS was used with slightly more porous fuel electrode, but comparable fabrication procedure. Detailed cell specifications for each test are outlined in Table 2.

***Table 2.*** *Cell and test specifications for long-term electrolysis test.*

| Test no | Test conditions | Cell specification | Test specifications |
|---|---|---|---|
| Test A | Inlet $p(H_2O)/p(H_2)$:0.85/0.15, air to oxygen electrode, 695 °C, -0.3 A/cm$^2$, 11 % conversion | Ni/YSZ ratio 40/60 | 10 kh steam electrolysis test (first 3 kh included in Figure 1). No re-cycling of gasses. |
| Test B | Inlet $p(CO_2)/p(CO)$:0.89/0.11, air to oxygen electrode, 695 °C, -0.3 A/cm$^2$, 14 % conversion | Ni/YSZ ratio 50/50 | $CO_2$ electrolysis, no re-cycling of gasses, $CO_2$ from central supply |
| Test C | Inlet $p(CO_2)/p(CO)$: 0.89/0.11, air to oxygen electrode, 695 °C, -0.3 A/cm$^2$, 14 % conversion | Sister cell to the cell in Test A | $CO_2$ electrolysis, re-cycling of gasses, $CO_2$ from central supply. |
| Test D | Inlet $p(CO_2)/p(CO)$: 0.89/0.11, air to oxygen electrode, 695 °C, -0.3 A/cm$^2$, 14 % conversion | Cell having a higher porosity in active fuel electrode (Ni/YSZ ratio 40/60) | $CO_2$ electrolysis, re-cycling of gasses, $CO_2$ from central supply. |
| Test E | Inlet $p(CO_2)/p(CO)$: 0.89/0.11, air to oxygen electrode, 695 °C, -0.3 A/cm$^2$, 14 % conversion | Ni/YSZ ratio 40/60 | $CO_2$ electrolysis, re-cycling of gasses, $CO_2$ from bottle. |
| Test H | Inlet $p(CO_2)/p(CO)$: 0.89/0.11, air to oxygen electrode, 695 °C, -0.3 A/cm$^2$, 14 % conversion | Ni/YSZ ratio 40/60 | $CO_2$ electrolysis, re-cycling of gasses, $CO_2$ from bottle. Inlet fuel gas cleaning. |

**Test conditions**

Five cell tests were conducted. Test A was the $H_2O$ electrolysis cell test from M1.1 and serves as a reference test, while test B-E were $CO_2$ electrolysis tests. The $CO_2$ feedstock gas was from the central supply for test B-D, while test E used $CO_2$ from a bottle. Test B was without re-cycling of gasses, while test C-E was with re-cycling. The specific conditions for each test are outlined in Table 2. For tests with recycling of gas, the electrolysis test was started with $CO_2$ and CO flow from a central gas supply and a container was first filled with the outlet gas mixture (pressurized) and then led to an extra mass flow controller in the test rig. The flow of outlet gas from the electrolysis process was then re-used, CO from the central supply was stepped down and stopped while the $CO_2$ supply was adjusted to reach the desired $CO_2$/CO ratio and conversion at -0.3 A/cm$^2$. Temperature and $pO_2$ inlet measurements where used to fine tune flow settings for $CO_2$ and re-cycled gas stream.

**Cell test results**

Figure 11 shows results from the long-term cell tests. The reference cell showed excellent stability, as described in more detail in section 1.5.2.1. However, tests conducted in $CO/CO_2$ suffered from severe degradation of the electrode ($R_P$ increase). Since cells running with recycled CO also degraded heavily, the impurities must originate from the $CO_2$ supply. Solving the issue by changing the cell manufacturer (from DTU to HTAS) and modifying the porosity of the fuel electrode was unsuccessful (Test D). Furthermore, changing the $CO_2$

source from the central supply to a bottle with different piping did also not resolve the issue (Test E).

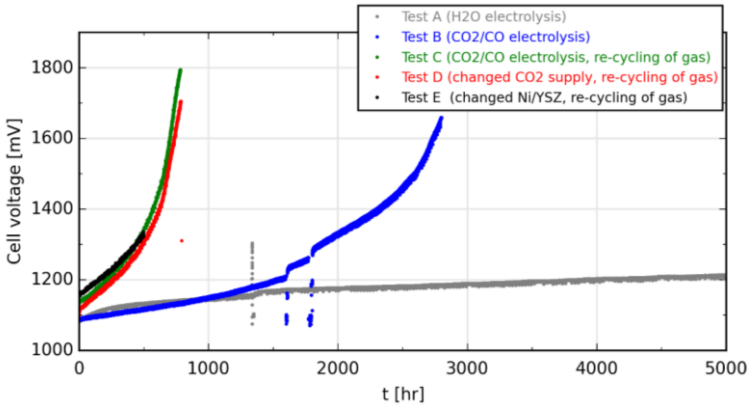


***Figure 11.*** *Cell voltage (top) development during long-term electrolysis test. Ohmic resistance stay constant throughout all of the test (as exemplified in Figure 14) and $R_p$ follows the trends as observed for the cell voltage curves.*

However, simple gas cleaning (based on crushed fuel electrode half-cell) of the inlet gas mixture to the fuel electrode had a noticeable positive effect on minimizing the fuel electrode degradation, as depicted in Figure 12, where Test H was operated at same conditions as previous tests, but applying gas cleaning. At around 1300 h of operation, an attempt to clean the gas cleaning powder was made, and at around 1700 h of test the gas cleaning powder was substituted with a fresh portion of crushed half-cell for gas cleaning.

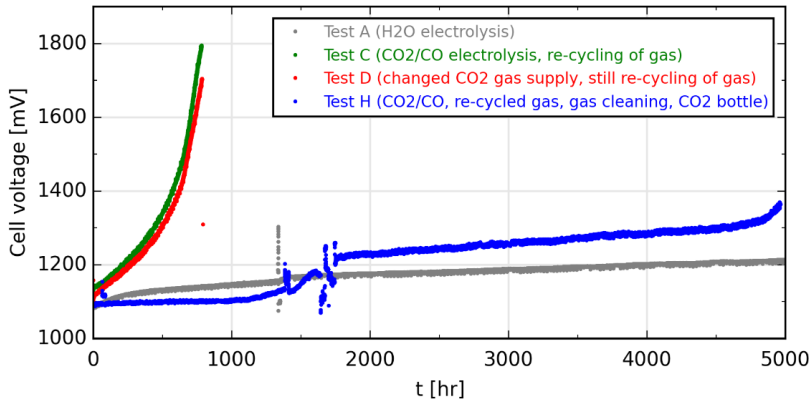


***Figure 12.*** *Cell voltage development during long-term electrolysis test at 695C and -0.3 A/cm$^2$. All $CO_2$ electrolysis test were operated at same test conditions, but for test H the fuel gas inlet was cleaned prior to feeding it to the SOEC.*

EIS were recorded during the presented long-term electrolysis tests. Figure 13 shows the EIS recorded at start of the galvanostatic long-term test for Test A ($H_2O$ electrolysis) and for Test C ($CO_2$ electrolysis with recycle). From CNLS fitting of the spectra, the fuel electrode resistance was estimated to 0.341 Ω cm$^2$, corresponding to a fuel electrode overpotential of 102 mV (assuming that the majority of resistance attributed to physical process, $R_{Gas\ diff.}$ and $R_{GasConv.}$ takes place outside the active fuel electrode layer). This fuel electrode overpotential is well below the reported suggestion for an overpotential-threshold, for which severe Ni migration can be avoided [7]. This is in agreement with the observed stability of the ohmic resistances over time. Likewise, the fuel electrode overpotential for Test A was found to be well below the threshold for severe Ni migration since the equivalent circuit model of EIS from start of Test A lead to a fuel electrode resistance of ~0.190 Ω cm$^2$, i.e. a fuel electrode overpotential of 57 mV.

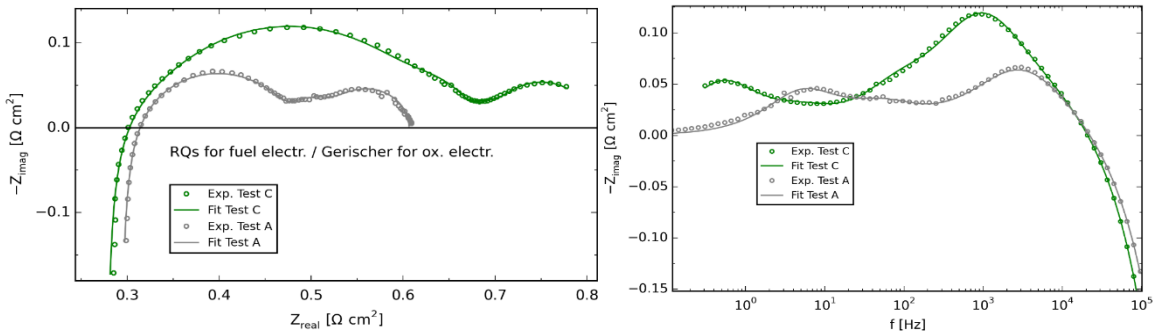


***Figure 13.*** *Nyquist and Bode plot (imaginary part) of experimental IS and corresponding equivalent circuit model fit for the first IS recorded during long-term electrolysis Test A ($H_2O$ electrolysis) and Test C ($CO_2$/CO electrolysis).*

Figure 14 shows the development from start to end of $CO_2$ electrolysis test C and H; i.e. with and without gas cleaning of the fuel inlet gas stream. Simple visual inspection of the EIS for test C given in Figure 14 indicates that the polarization resistance attributed to electrochemical reactions has increased to ~1.75 Ωcm$^2$, corresponding to an overpotential of 525 mV.

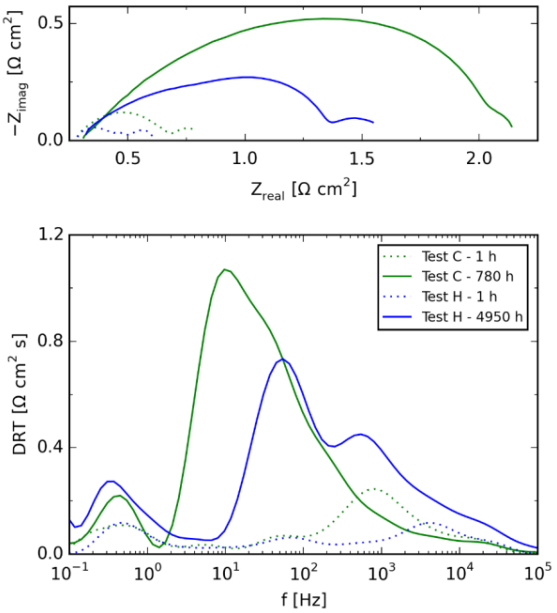


***Figure 14.*** *Nyquist and DRT plot of impedance spectra recorded at 1 h and end of test, i.e. 780 h of test for test C (re-cycling of gas) and 4950 h of electrolysis test for test H (re-cycling and cleaning of inlet gas). Identical $CO_2$ electrolysis test conditions (695C and -0.3 A/cm$^2$).*

**Post-mortem microscopy**

Post mortem analysis was performed via scanning electron microscopy (SEM) and Raman spectroscopy for selected samples after the long-term tests. SEM was performed as described elsewhere in this report. For Raman spectroscopy a Renishaw InVia Reflex Spectrometer system was used with a 532 nm laser, exposure time 20 s, laser beam spot size on the sample 1 μm and laser power <8 mW. Fractured cross sections of the cells were investigated during the Raman spectroscopy without any further treatment.

During post-mortem analysis of the cells with high degradation, an increased pore fraction in the inner most 4-6 μm in the inlet piece (Figure 15b) was observed. This can be due to onset of Ni migration [6,7,12] while the region closer to the interface between the fuel electrode and the anode support layer appear densified. These effects were less noticeable for the outlet piece.

Another perhaps more detrimental observation was made. A weakened interface and significant delamination between the electrolyte and the fuel electrode was observed, as

shown in Figure 15. A weakened interface is not necessarily delaminated during test (where it is kept at high temperature and with mechanical load), but can delaminate upon dismounting of the cell from the cell test housing. The delamination of the fuel electrode from the electrolyte was not observed during microscopy of Test A nor reported for several other long-term steam electrolysis tested cells [6,7,12], but was observed by Skafte et al. for even shorter $CO_2$/CO electrolysis test [9]. This suggests that the observed delamination for e.g. the cell from Test B and Test C is not due to improper manufacturing nor duration of test, but rather seems to be caused by carbon deposition. The high electronic conductivity of carbon nanotubes between the electrolyte and the fuel electrode could also explain the steady ohmic resistance during testing. Notice however, that the SEM images in Figure 15 do not provide direct evidence of carbon deposition. To investigate possible carbon deposition in the tested cells, Raman spectroscopy was obtained on pieces of cells from Test B, Test C and Test H.

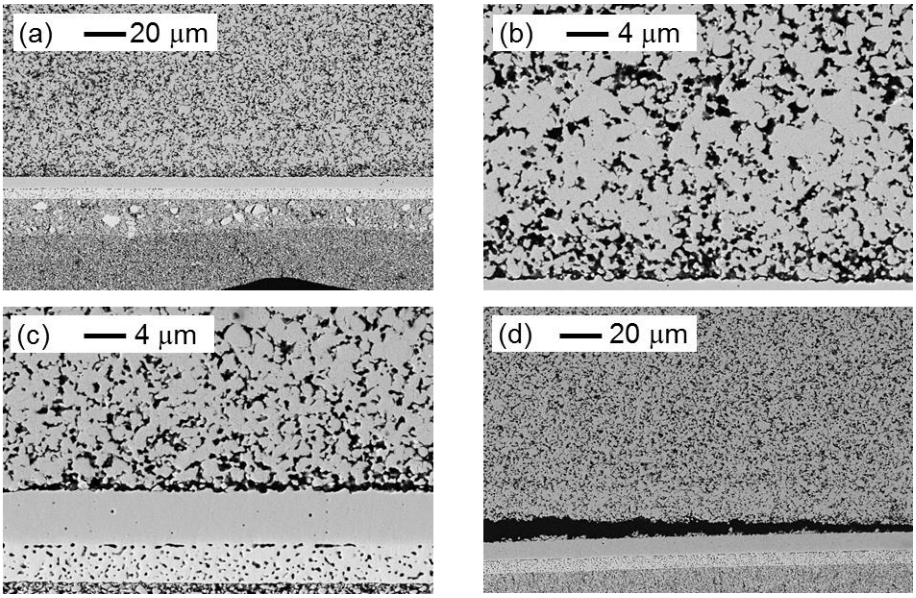


***Figure 15.*** *SEM images of fuel inlet piece of cell from Test B (a), higher magnification image of fuel inlet piece of cell from Test B (b), higher magnification image of fuel outlet piece of cell from Test B (c) and overview SEM image of the middle part of the cell from Test C (d).*

Figure 16 provides an example of a Raman spectrum recorded in the active fuel electrode for the cell from Test C. For Test C, Raman spectra were recorded in both the oxygen electrode, the barrier layer, the electrolyte, the fuel electrode and the fuel electrode support layer of the cell. For this test, five different points were investigated in the fuel electrode, and all points showed clear signs of carbon depositions, evidenced by peaks at 1345 $cm^{-1}$, 1585 $cm^{-1}$ and 2684 $cm^{-1}$, which can be assigned to disordered graphite (D), ordered graphite (G) and the overtone of the D peak (2D) respectively [13,14]. In contrast, none of the other layers in the test C cell showed evidence of carbon formation, confirming that the carbon formation is taking place in the fuel electrode area only. Additional Raman analysis with higher spatial resolution showed that the inlet part of the fuel electrode had the highest carbon peaks intensity and extended ~10 µm into the electrode. In the middle of the cell, the carbon peaks intensity was lower, but carbon extended ~20 µm into the electrode, as seen in Figure 17. Contrary to expectations, the outlet part of the cell showed the least amount of carbon and only extended ~5 µm into the electrode. A tentative explanation could be that the inlet part of the cell is exposed to the highest current density and a concentrated deposition at the fuel electrode|electrolyte interface takes place. In the middle of the cell, where temperature and current density is lower, and CO concentration is higher, the deposition is more wide-spread into the electrode.

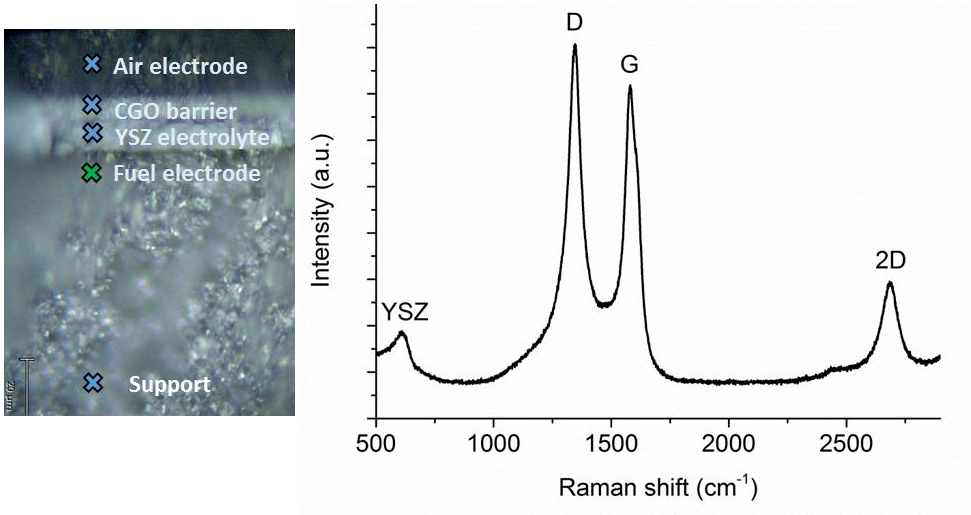


***Figure 16.*** *Raman analysis in different spots along the cross-section of the cell. The spectrum shows the active fuel electrode, where a significant signal from D and G band carbon is seen, proving the deposition of carbon.*

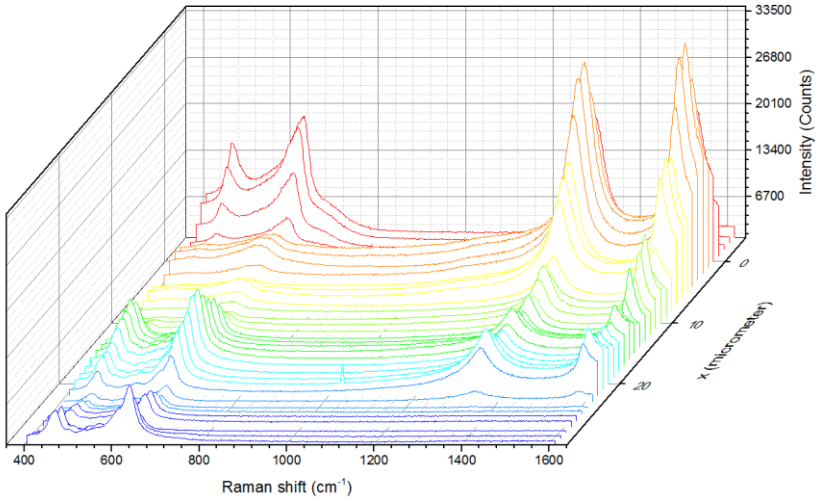


***Figure 17.*** *Raman spectra collected from the middle of cell C, starting from the electrode|electrolyte interface (x = 0) and throughout the electrode.*

Carbon deposition only in the active fuel electrode along with the significant increase in fuel electrode overpotential, as shown earlier, suggests that the detected carbon is correlated with high local overpotential. Correlation with cell overvoltage was also shown in Figure S1 and Figure S7 in Skafte et al. [9]. The externally set test conditions, i.e. inlet gas composition and average cell temperature of 11% CO and 695 °C, respectively, were far from the threshold for carbon deposition (i.e. 59% CO at 695 °C) and in a previous stack test conducted by HTAS, it has been possible to operate at these externally set test conditions. However, local test conditions were most likely in the regime for carbon deposition. A fuel electrode overpotential of 525 mV, as shown earlier for end state of cell B and C, far exceeds the theoretical threshold of the Boudouard reaction. Considering only the resistance contribution attributed to the charge transfer reaction, $R_{Ni/SZ,TPB}$ = 0.274 Ω cm$^2$, for Test C at the start of the test, this resistance contribution correspond to an overpotential of 82 mV. Using FACTSAGE® software the calculated carbon-deposition overpotential threshold should be of ~106 mV (700 °C, inlet gas conditions) or ~102 mV (700 °C, outlet gas conditions). This indicates that the overpotential for test C might locally already reach the carbon deposition threshold; also considering the presence of resistance contribution from the ionic "rail" in the fuel electrode that was estimated to be $R_{YSZ,ionic}$ = 0.067 Ω cm$^2$ at start of test C. Importantly, even a limited fuel electrode degradation e.g. caused by gas phase impurities will increase the electrode overpotential above the calculated theoretical

threshold for carbon deposition. We suspect that impurities in the gas stream are sulfur-based compounds. Such trace impurities have previously been shown to cause tremendous degradation for the Ni/YSZ based fuel electrode even when added in the ppm- or ppb range [9]. Thus, if even minute amounts of sulfur compounds are present in the inlet gas or the gas tubing, the significant degradation of the fuel electrode on account of this would quickly lead to the even worse mechanism of carbon deposition. In this perspective, this work exemplifies that Ni/YSZ based SOECs are order(s) of magnitude more sensitive towards sulfur-based impurities compared to SOFC operation of similar cells [15,16].

Post-mortem analysis via SEM for test H does not show sign of delamination between the fuel electrode and the electrolyte as it was observed e.g. for test B and C, not even in the fuel inlet part of the cell as depicted in Figure 18. Furthermore, Raman analysis showed no significant carbon peaks. This indicates that severe carbon deposition did not take place in this part of the fuel electrode. However, it was noted that the part of the electrode closest to the electrolyte appeared more porous than the outer part of the electrode and more porous than for a similar reference cell. This could indicate that Ni migration has initiated, though not yet to an extreme degree as seen for other long-term tested SOECs [6]. A fast check of possible Ni migration was performed via EDS analysis in the selected regions as indicated by yellow squares in Figure 18 for a couple of regions in the fuel inlet part of the cell each covering an interface length of 100 μm. The quantification of the EDS led to atom percentage ratios Ni/(Y+Zr) of 0.74 for the inner part of the electrode, 1.11 for the outer part of the active fuel electrode and 1.15 for the support layer with an estimated error of ± 0.05 for the ratios.

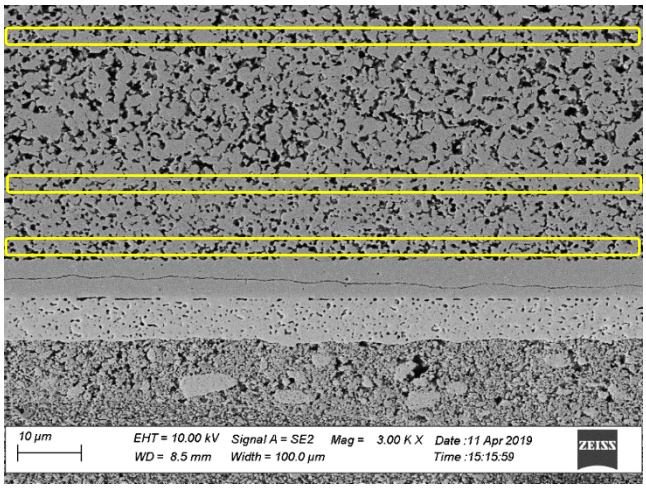


***Figure 18.*** *SEM image of fuel inlet part of cell from test H. Yellow squares mark region for EDS mapping, i.e. inner part of active fuel electrode, outer part of fuel electrode and further out in the support layer of the cell.*

**Conclusions**

Based on the cell test results, impedance spectroscopy and postmortem analysis (SEM and Raman spectroscopy) we conclude that SOEC are highly prone to carbon deposition even at relatively mild conditions causing severe degradation of the cells. Similar externally set test conditions for steam electrolysis lead to very stable performance over 10 kh electrolysis when testing a sister cell. For the $CO_2$-electrolysis test in this work, fast and severe increase of fuel electrode overpotential (analyzed via IS), e.g. initiated by even ppb level of sulfur impurities, was observed and this provided test conditions enabling carbon deposition even though the externally set test conditions were clearly out of the theoretically calculated carbon deposition range. Carbon deposition in the active electrode was confirmed via Raman spectroscopy and only detected in the active fuel electrode layer. Cleaning of the $CO_2$/CO inlet gas stream had tremendous and positive effect on the long-term durability.

***M1.4: Cells with improved lifetime developed, produced, and delivered to WP2 for stack testing.***

Two routes were followed for improving lifetime. One was an attempt to mitigate Ni migration by doping the active fuel electrode with $Al_2TiO_5$, and another was a more radical redesign of the state-of-the-art cell with steel acting as the supporting material rather than the ceramic fuel electrode. These activities are still under development and will continue in future projects, which also means that optimized cells were not produced in time for delivery to stack testing in WP2.3. Moreover, sine the new cell design is looking promising, the concept is under consideration for a patent application. This was however not filed in time for publication of this report and is hence omitted here.

**$Al_2TiO_5$ doping of Ni/YSZ fuel electrode**

Based on previously reported results on Ni depletion, i.e. Ni migration away from the fuel electrode/electrolyte interface upon long-term SOEC tests, an important aspect of improving long-term stability of S-o-A SOEC fuel electrode is to hinder this degradation mechanism [6,7]. Inspired by previously reported work by Kishimoto and co-workers on the effect of $TiO_2$ doping on Ni wetting angle and agglomeration behavior on stabilized zirconia substrates [17] and the work by Law and Sofie on anchoring Ni by addition of aluminum titanate via infiltration [18]; it was decided to attempt to improve the stability of the fuel electrode by adding 2 mole% $Al_2TiO_5$ to the active fuel electrode. $Al_2TiO_5$ doped half-cells were produced. However, it was not possible to sinter the CGO barrier layer on the multilayer half-cell as is normally performed. Several sintering temperatures were tried without successful adhesion of the CGO barrier layer. Finally, it was decided to add the LSC/CGO oxygen electrode directly on the electrolyte and sinter without a barrier layer.

A standard electrochemical characterization test was performed on the $Al_2TiO_5$ doped cell. The very first impedance spectrum at 850 °C, air and 4% $H_2O$ in $H_2$ led to an ohmic resistance of 0.05 $\Omega cm^2$ (acceptable ohmic resistance, and expected considering the relatively thin electrolyte and lack of CGO barrier layer) and a total polarization resistance of 4.91 $\Omega cm^2$. For comparison; a similar non-doped cell tested at the same conditions in the same test-rig had ohmic and polarization resistance of 0.08 $\Omega cm^2$ and 0.41 $\Omega cm^2$, respectively. Furthermore, a current of only 0.13 $A/cm^2$ could be drawn during the first iV-curve, and the cell degraded further during the initial electrochemical characterization.

Figure 19 shows SEM images of the cell after initial characterization. A proper fuel electrode structure was obtained as well as proper layer thicknesses. In Figure 19a, encircled particles have been investigated via EDS and are all alumina particles. However, no traces of titanate could be detected via EDS neither in the alumina particles nor in other parts of the active fuel electrode. Due to the problems with sintering and adhesion of the CGO barrier layer, the interface between the electrolyte and the oxygen electrode was also investigated by EDS. This is marked by the red square in Figure 19b. EDS in this interface could detect no Ti-species. In conclusion, it was not possible to locate Ti-species after sintering and testing, and the detected alumina-species do not seem to contain titanium either. The beneficial effect was not obtained, and further attempts were abandoned. It is noted, however, that it may be possible to keep the migrating Ni in place by infiltrating $Al_2TiO_5$, instead of doping the electrode. Such experiments are suggested for future projects.

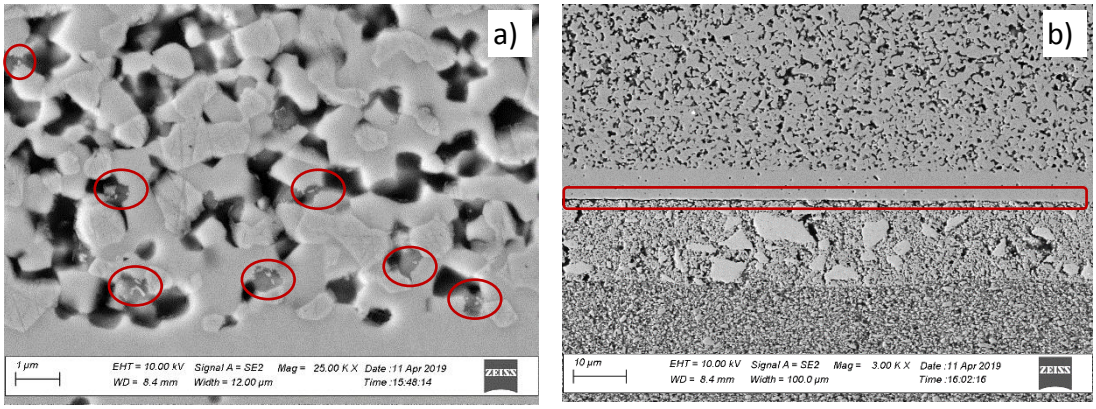


***Figure 19.*** *SEM images of the cell with 2 mole% $Al_2TiO_5$ added to the active fuel electrode. a) A zoom-in on the active fuel electrode and its interface towards the YSZ electrolyte. Red circles mark examples of alumina particles (no titanate) in the structure. b) Overview image of the cell where the red square mark the electrolyte-oxygen electrode interface investigated by EDS in search of Ti-species.*

### *1.5.3 WP2: Mitigating critical degradation mechanisms in stacks*

The three main tasks of WP2 was to conduct performance mapping of stacks during SOEC operation using EIS (WP2.1), perform long-term testing and determine end-of-life criteria on stack level (WP2.2), and finally, develop an improved stack design and operation profile for enhanced reliability and lifetime (WP2.3).

#### 1.5.3.1 WP2.1: Performance mapping of stacks during SOEC operation using EIS

To mitigate degradation mechanisms on stack level it is crucial to obtain better diagnostics tool to pinpoint said mechanisms. This was successfully attempted in WP2.1, where electrochemical impedance spectroscopy was carried out on a large 75-cell HTAS stack.

***M2.1: Extended stack testing protocol with impedance spectroscopy developed and tested on a large (>40 cell) stack***

**Introduction**

Increasing the value output of an experiment is always of high importance. Especially so when expensive stack testing is carried out. In WP 2.1, EIS on individual cells in a large HTAS TSP-1 stack was carried out successfully. The method for doing so was developed previously at DTU Energy [1,2], and has in this project been optimized and further developed. One of the main objectives was to analyze the data for signs of contact issues within the stack. This has been a long-standing issue for the technology in general, as reported under WP1.2 (section 1.5.2.2).

As shown in Figure 20 (Left), the stack is mounted in a stack testing rig with a furnace, gas supply and mechanical load. Voltage and current is measured and supplied to the end-plates of the stack, and connected to a stand-alone trolley (Figure 20 (Right)). Moreover, a number of voltage wires are connected to interconnects between individual cells, enabling measurements across the interconnects and single cells (repeating units, RUs) as well as cell groups. Voltage and EIS was measured for 51 RUs, and 4 cell groups of 6 RUs each, totaling 75 cells.

***Figure 20.*** *(Left) Photo of mounted TSP-1 stack, with voltage wires. (Right) Photo of transportable EIS trolley*

**Stack characterization**

To confirm nominal performance, the OCV (Figure 21 (Left)) and voltage under current load (Figure 21 (Right)) of the cells was analyzed. The average values were within specifications, but a significant outlier is RU75 with about 50 mV lower voltage under 25 A load (SOFC mode).

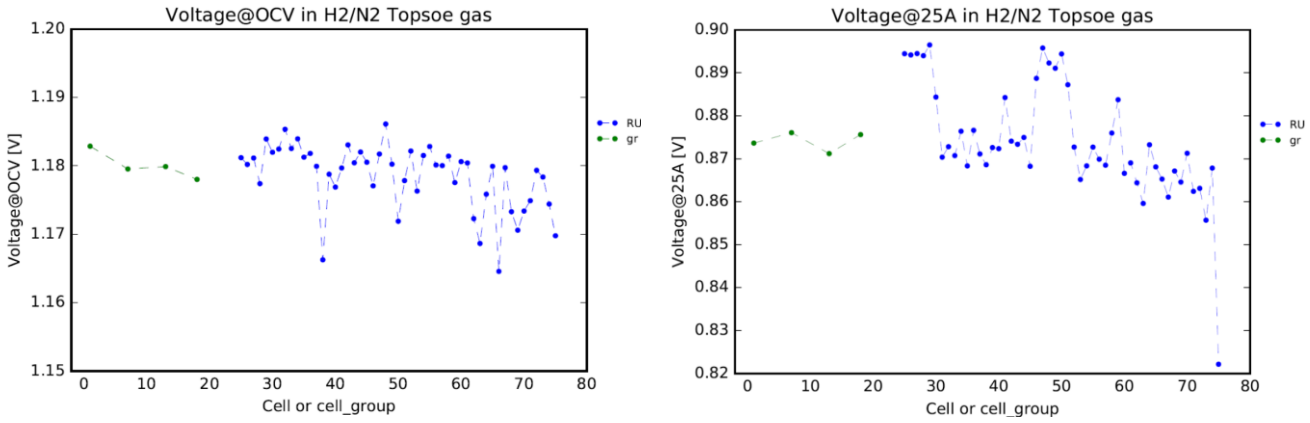


***Figure 21.*** *(Left) Voltage measurements at OCV. (Right) Voltage measurements under current load of 25A.*

Subsequently, EIS were measured at three conditions (Table 3).

***Table 3.*** *EIS conditions during stack characterization in both SOFC and SOEC mode.*

| **Condition** | **Fuel gas** | **Oxygen gas** | **Temperature** |
|---|---|---|---|
| A | $H_2$:$H_2O$ 80%:20% | Air | 700 °C |
| B | $H_2$:$H_2O$ 80%:20% | $O_2$ | 700 °C |
| C | $H_2$:$H_2O$ 10%:90% | Air | 700 °C |

After correcting for some of inductance caused by the measurement setup, the EIS is plotted as a Nyquist plot in Figure 22(A)-(C).

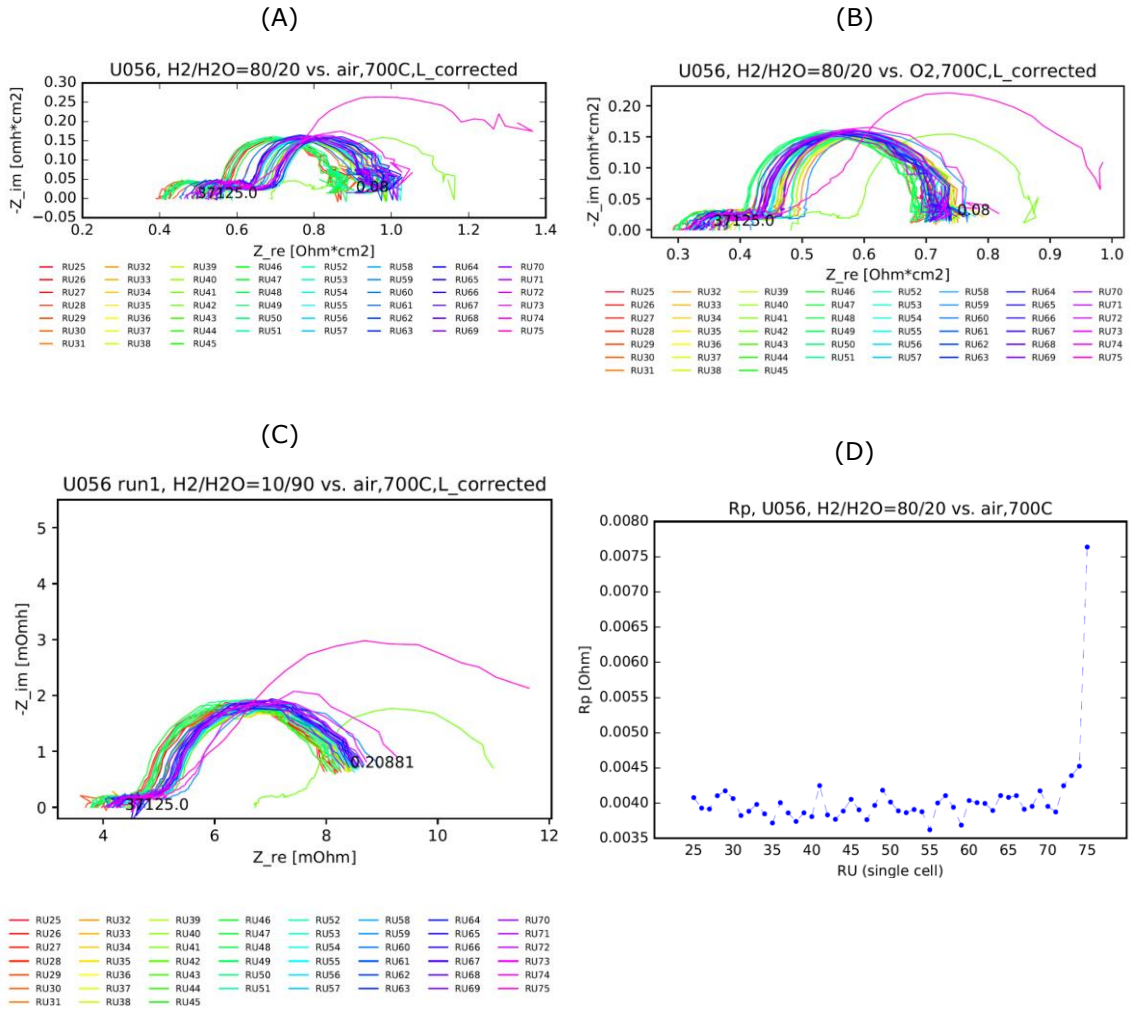


***Figure 22.*** *(A) Nyquist plot for condition A. (B) Nyquist plot for condition B. (C) Nyquist plot for condition C. (D) Quantified polarization resistance of each RU for condition A.*

As seen, there is a considerable spread in Ohmic resistance, $R_S$, between 0.40-0.55 Ω cm$^2$ and 0.30-0.40 Ω cm$^2$, for air and $O_2$, respectively. First of all, the spread makes you suspect differences in contacting between the different RUs. Second, the difference from air to $O_2$ is peculiar, as one would not expect this. It could point to differences in contacting and/or conductivity for the oxygen electrode. The temperature profile inside a stack is not homogeneous, which will generate temperature gradients affecting the local conductivity of individual cell/stack components.

Polarization resistance, $R_P$, is very similar for all RUs, except RU75, as seen in Figure 22(A) and Figure 22(D). The large $R_P$ of RU75 and similar $R_S$ as the other RUs indicate that the issue is not contacting, as $R_S$ and $R_P$ would scale with the lower area being contacting. Conversely, the other outlier in the middle of the stack, has a higher $R_S$ and similar $R_P$, again indicating that the effect does not have to do with area lost. The higher $R_S$ could instead be due to lower conductivity of the electrodes or the interconnect/coating.

**Comparison of conditions**

By plotting the imaginary part against the frequency, a so-called Bode plot, one can display resistance changes in various frequency ranges for changes in testing conditions. The difference between condition A and B is an oxygen gas change (Figure 23(A)), which reveals the contribution of the oxygen electrode and diffusion resistance of the oxygen electrode. The main peak at ~3000 Hz is higher than expected for the oxygen electrode, and there does seem to be a contribution at lower frequency, which represents gas diffusion and conversion resistance.

Similarly, a fuel gas change Bode plot is shown in Figure 23(B). The main peak is observed at ~5000 Hz, corresponding to the electrochemical contribution to the resistance of the fuel electrode.
By plotting $R_S$ for the three different conditions (Figure 23(C)), we see a lower resistance when flowing $O_2$ to the oxygen electrode, as expected. The difference is however not as significant as when changing the fuel gas from 20% $H_2O$ in $H_2$ to 90% $H_2O$ in $H_2$ (Figure 23(D)). This indicates that the main resistance contribution is coming from the fuel electrode.

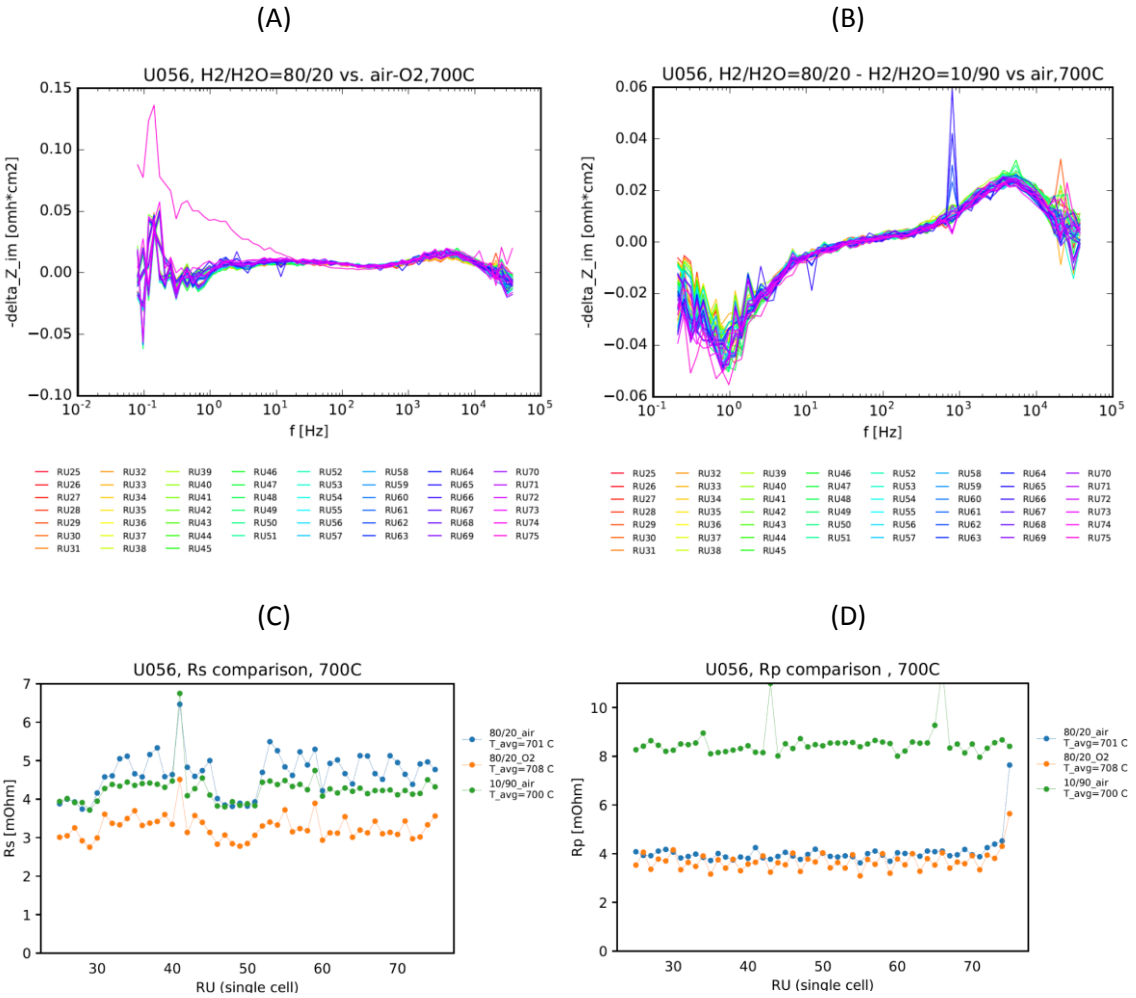


***Figure 23.*** *(A) Delta Bode plot of condition A and B, oxygen gas change. (B) Delta Bode plot of condition A and C, fuel gas change. (C) Comparison of RS for all three conditions. (D) Comparison of RP for all three conditions.*

**Conclusions**
A large TSP-1 stack with 75 cells was tested with EIS characterization, and the milestone was accomplished. A stand-alone trolley with the EIS equipment was built, which will be of great use for future stack testing in other projects. The data obtained was optimized by correcting for inductance.

### 1.5.3.2 WP2.2: Long-term testing and end-of-life criteria on stack level

***M2.2: Report on End-of-Life criteria***

From a commercial perspective it is highly useful to have a clearly defined End-of-Life criteria, where the system must be shut down. This is however not easily obtained with limited SOEC data at the moment, but a prerequisite is an elucidation of potential degradation and failure mechanisms.

**Introduction**

An important goal of WP2 is to define relevant end-of-life criteria for a stack operating in electrolysis mode. As long as the solid oxygen electrolysis cell (SOEC) stack is producing gas (i.e. CO and/or H2) and there is no mechanical failure then the stack can be considered "operational". However, there are limits for stack operation conditions, beyond which the stack is "unhealthy" or "about to fail". Knowing these limits is crucial for better planning of maintenance operations in future commercial SOEC systems.

HTAS has two sets of clear criteria for an SOEC stack that can pass the criterion of acceptable operation. One is that the *performance must be constant*, i.e. a specified power (a given number of Watts) put into the stack must give at least the production rate of CO and/or $H_2$ that was promised. This is in practice done by *starting the stack life at 700 °C* and then use increasing temperature to compensate the degradation. The *end-of-life criterion is now set as reaching 825 °C*, because above this temperature the interconnect plates of ferritic stainless steel will oxidize very fast, and full oxidation of the interconnector plate means that the stack has been destroyed.

Another criterion is *quality of CO*, which is paramount in chemical industry application with on-site production of CO. This means that mechanical integrity is most important, i.e. almost no cracks or holes in the electrolyte, the interconnector plates or the seals can be allowed. With eCOs™ HTAS offers from 99.0 % up to 99.999 % CO depending on the customer's needs. "Standard" is *99.0 % and 99.5 % CO*. As it is not possible to electrochemically reduce all $CO_2$ in the gas stream to CO without precipitating carbon, the unconverted $CO_2$ must be removed by physical-chemical methods.

As air or $N_2$ may be used as sweep gas on the oxygen side, it is possible to calculate the allowed leak rate of air and/or $N_2$ though the electrolyte, the interconnect, and the sealings, when the maximum accepted level of $N_2$ in the CO product gas has been decided.

Recent DTU and HTAS reviews on general degradation mechanisms and measures to prevent and repair degradation has been published by Graves [3] and Skafte [4]. These works are in particular relevant to HTAS stacks. The stack type that we in particular have in mind in this summary, is the HTAS TSP-1 type, which is a bipolar plate type with Ni-YSZ supported cells. The SOEC bipolar flat plate stack must be able to convert the reactant gases ($CO_2$ and/or $H_2O$) and electrical energy into CO and/or $H_2$.

It is important to note that an SOEC stack should run as close to thermoneutral condition as possible, i.e. as close as possible to the thermoneutral cell voltage, $E_{tn}$, which is in the range of 1.3 V to 1.5 V. The exact value depends on the operation conditions including the composition of the feed i.e. $CO_2$ or $H_2O$ with a low concentration of CO or $H_2$ or a mix of all of them [5]. The reason for this is that the closer the operation cell voltage is to $E_{tn}$, the healthier self-cooled is the stack, and the lower is the temperature gradient, and this decreases the probability of cell cracks caused by thermal stresses.

**Cell degradation**

The degradation rate depends for a given cell and gas reactant mainly on the cell voltage/current density. The electrode potential vs. a well-defined reference is the main parameter that describes the thermodynamic state of a given electrode under given conditions. The $Pt/O_2$ (1 atm. $O_2$, temperature) electrode is recommended as the common reference electrode for SOC electrodes, even though these electrode potentials are usually not directly available, but have to be calculated from electrochemical characterization of a cell [6]. Recent tests have proven that the outcome of durability results is dependent on the test mode (galvanostatic or potentiostatic) [7]. This is a consequence of the importance of the electrode potential as explained below. Furthermore, alternating reversal of the current, i.e. changing the test mode from electrolysis to fuel cells forth and back, may almost stop the cell degradation, see below.

At very positive potential the Ni is oxidized to NiO, which initially is formed as nanoparticles. In a kind of analogy the reduction case, a slow, short oxidation this may temporarily activate the

electrode. If the oxidation is continued this will damage electrode; especially if the reduction-oxidation of Ni happens many times (redoxing), the cermet will be mechanically destroyed, because of the big volume changes associated with the oxidation of Ni in combination with the fact that fast self-diffusion of Ni causes the Ni particle to coarsen and redistribute inside the Ni-SZ cermet.

**Electrode Potential Driven Loss of Contact**

This type of degradation is typically taking place within the first 1000 h of test at current densities above around 1 A $cm^{-2}$ in good cells, i.e. Ni-YSZ electrode at potentials in the range of ca. -1.2 to -1 V vs $Pt/O_2$ (1atm., 800 °C). The phenomenon is summarized below. It is described in more details in [8,9]. However, the possible threshold value, above which this occurs, is not well determined, and more work on this is definitely needed.

Figure 24 shows the appearance in SEM pictures of the Ni-YSZ electrode part next to the electrolyte. It displays the structure of a non-tested electrode, of an electrode at gas inlet and outlet after tests during 678 h and of one at inlet and outlet after 138 h at -2.0 A $cm^{-2}$ in co-electrolysis mode. Our hypothesis is that the Ni migration starts due loss of contact between Ni and YSZ particles. The loss of contact is assumed to be caused by positive free energy of formation of Ni-YSZ interfaces in the most polarized part of the Ni-YSZ electrode. This may happen at potentials above or below the zero charge potential, which seems to be in the vicinity of OCV of the Ni electrode material at OCV in $H_2$-$H_2O$ gas mixtures at typical SOC operation conditions. If $\Delta G_{if}$ is positive then the contact will not be stable, and the Ni-YSZ contact will be gradually lost over time.

When the Ni-YSZ contact is lost then the Ni will start migrating, which will cause a loss of contact between Ni particles. Further, the positive $\Delta G_{if}$ may cause a Ni particle shape change towards ball shaped Ni particles, and this will also contribute to loss of Ni – Ni contact. A similar phenomenon is seen in fuel cell mode on the positive side of OCV in potential range of approximately the same numerical range of overpotential. Finally, there are indications that the loss of Ni-Ni contact may be accelerated by the influence of impurities.

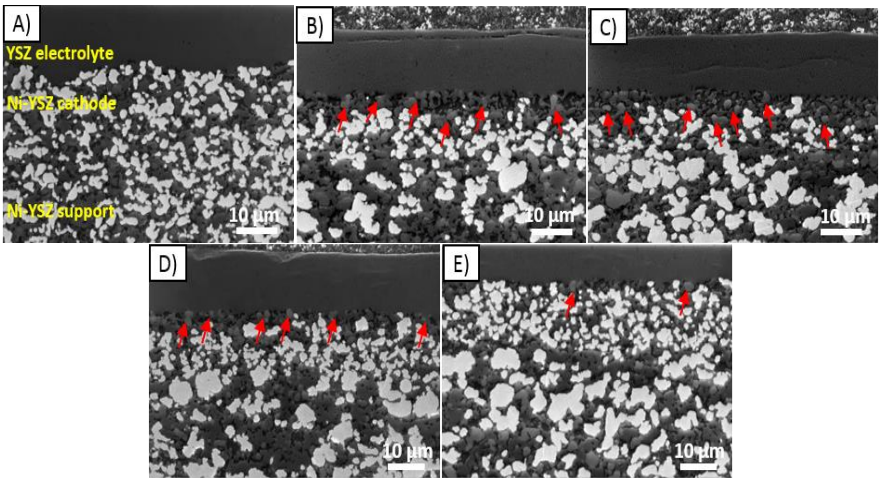


***Figure 24.*** *Low-voltage SEM micrographs of Ni-YSZ 8YSZ electrolyte. A) not tested, B) $H_2O$-$H_2$ inlet and C) outlet tested 678 h, D) inlet and E) outlet tested 138 h. Bright: interconnected Ni; light grey: non-connecting Ni; dark grey: YSZ; black: pores. Red arrows point to uncontacted Ni. 865°C increasing to 875 °C. Inlet gas: 45 % $H_2O$ + 45 % $CO_2$ +10 % $H_2$, -2.0 A $cm^{-2}$, 60 % (steam + $CO_2$) conversion.*

**Carbon formation in the Ni-YSZ electrode**

The chemistry/electrochemistry of $C/CO/CO_2$ system is relative complicated as shown in Figure 25, which gives potentials and overpotentials at which carbon deposition may/or may not take place [10]. Here it is noted that it is definitely not enough that the average composition is in the carbon free regime. The conditions in every local point must be at conditions that will not precipitate carbon. Thus, especially in the bottom of pores in the electrolysis cathode beneath the support layer, there is a risk of precipitation of carbon in the

Ni-YSZ active electrode layer. This means that it is necessary to have operation conditions with a significant margin to any carbon precipitation, or an experimental "calibration" of the cell stack in question has to be carried out. Experimentally precipitation of carbon in Ni-YSZ-electrodes has been observed in SOCs with too little porosity in the Ni-YSZ support layer [10-12].

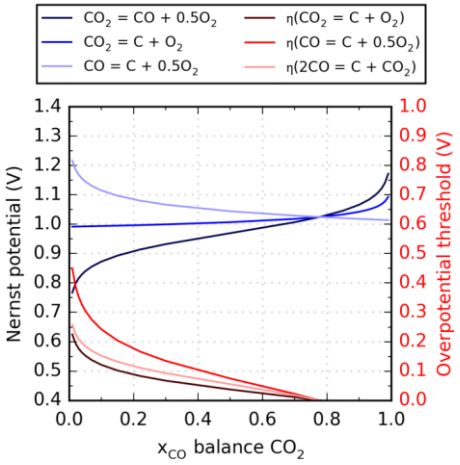


***Figure 25.*** *Numeric Nernst potential (vs. Pt/air, 1 bar, 750°C) and overvoltage thresholds for $CO_2$ electrolysis at 1 bar CO + $CO_2$ and 750°C, and possible carbon formation reactions as a function of CO fraction under changing concentration of CO in $CO_2$. Shown are data for the $CO_2$ to CO electrolysis reaction and for the electrochemical carbon formation from either $CO_2$ or CO. The second y-axis gives the overpotential threshold for the two electrochemical carbon formation reactions and for the Boudouard reaction. From [10].*

Carbon precipitation and fiber formation (carbon nanotubes, CNT) will take place in Ni-YSZ cermets in hydrocarbon atmospheres in the whole temperature interval relevant for SOFC [13]. This shows that Ni is very prone to carbon deposition as soon as this is thermodynamic possible. Thus, if the $CO/CO_2$ ratio in the bulk gas predicts carbon deposition then it happens. The carbon precipitation limit may be passed locally even in cases, where the bulk $CO/CO_2$ ration if there is high diffusion limitation due to low porosity in the support layer such carbon destroys the Ni-cermet mechanically.

It has been shown that a Cu - gadolinia doped ceria (GDC) electrode is very tolerant to carbon deposition, and no carbon fibers are formed [14]. However, the mechanical integrity of Cu-cermets is not good at temperature above 700 C, because Cu tends to migrate into big lumps on the surface of the electrode. Thus, experiments with doped ceria as electrode on its own was performed (unpublished DTU results) and with Ni covered with doped ceria [15]. In both cases a significantly decreased carbon precipitation rate was observed and no detrimental carbon fibers were formed. Yet, the doped ceria electrode passivates due to carbonate and carbon formation on the surface (unpublished DTU results).

**Degradation of perovskite oxygen electrode**

At high positive potentials $O_2$ bubble formation in grain boundaries with weakening of YSZ near LSM at "high" oxygen electrode overpotential occurs [16]. Here "high" overvoltage is actually less than 60 mV at 850 °C.

Reactions between La and Sr based perovskite oxygen electrodes and YSZ is well known. Even in the case, where a reaction barrier of GDC is put between the YSZ and the perovskite, it is observed that the $Sr^{2+}$-ions diffuse through the grain boundaries of the GDC and form over long operation periods local volumes of non-conducting $SrZrO_3$, which is connected with a slow degradation. There is also a lot of literature about passivation of $O_2$ model electrodes due to segregation of SrO and $La_2O_3$ to the perovskite surfaces, but to which extent this is a valid for good composite electrodes consisting of a stable structure with nano-sized particles, remains to be determined. Actually, the status is that our best oxygen electrodes have a polarization resistance well below 0.1 $\Omega cm^2$ at 750 °C and the $O_2$ electrode degradation

seems not really to be an important problem at moderate polarization if only clean sweep gases are used.

**Poisoning of electrodes**
Small amounts of $SiO_2$, S and P have been reported to cause serious poisoning of both $CO/H_2$- and $O_2$-electrode. Furthermore, all known $O_2$-electrode types are sensitive to Cr(VI)-oxide or –oxyhydroxide vapor. The impurities may originate from either the raw materials of the electrode itself, from evaporation of other stack components or from impurities in the feed and sweep gases. The only measures against such poisoning are either to clean the materials and gases or to passivate the impurities by "scavengers".

In similarity with the carbon precipitation, doped ceria has been found to be much less prone to sulfur poisoning than Ni [14]. It seems that this is - to at least some extent - due to formation of Ce-O-S compounds and more data for the long term resistance of ceria electrodes towards relative high concentrations of S-compounds is needed.

**Stack degradation**
Apart from the cell degradation problems, an SOEC stack may also suffer from degradation of the stainless steel interconnect and gas distributors by high temperature oxidation, from degradation of the sealings and from thermo-mechanical degradation/ cracking of cells and glass sealings. Naturally, it is possible to protect the steel by coating with suitable ceramics or metals. For all three issues it applies that at the moment when the selection of steel and coating, cell type and stack design have been selected, then the only operational parameters that are important, are temperature and temperature gradient. The best tool to help with performing a stack operation as gentle as possible, is a computer implemented good mathematical model. Thus, the further discussion of how to optimize the durability of the stack materials does not belong to this summary.

**Conclusions**
The first remark is that, regrettably, we do not have sufficient data yet in order to set up clear thresholds for SOEC operation parameters, which will keep stack degradation below a predicted low degradation rate of say 0.2 %/kh.

The next remark is that the progress in understanding SOEC R&D at DTU and HTAS is in good progress. This is also the case internationally. The observations on the Danish cell reported above have later been confirmed, on the qualitative and semi-quantitative level, by other laboratories on cells and stacks produced by different companies [17].

A very encouraging finding in our research is that the most important parameter regarding degradation is the electrode potential. This in turn means that all improvements of electrode kinetics though improvements of electrode structure and composition means higher current density (CO production rate) without higher degradation rates.

***M2.3: At least 3 stacks tested for >1000h (input and validation of 3D models)***

During the first phase of the project HTAS tested four different TSP-1 stacks in $CO_2$ electrolysis in order to validate the 3D stack model and to evaluate different experimental design modifications to specific stack components. The stacks (full-sized 75-cell TSP-1.X stacks, where X is assigned to a specific generation in HTAS' stack production) and the included modifications are listed in Table 4.

The results from the first 2000h of testing is shown in Figure 26, including a reference stack from a previous project (ForskEL 2015-1-12276). All stacks were tested in $CO_2$ electrolysis at 50A, 30% conversion, with 750°C as inlet temperature. Air was supplied to the oxygen side.

***Table 4.*** *Summary of stacks tested in $CO_2$ electrolysis to achieve M2.3.*

| Stack-ID: | Stack gen.* | Modification | Total run time (h) |
|---|---|---|---|
| U-048 | TSP-1.3 | Modification to coating on interconnect (fuel side) | 2000 |
| U-049 | TSP-1.3 | Modification to coating on interconnect (fuel side) and contacting on fuel side | 2600 |
| U-070 | TSP-1.3 | Modification to coatings on interconnect (fuel side + air side) | 650 |
| U-071 | TSP-1.3 | Modification to coatings on interconnect (fuel side + air side) | 10000 (test ongoing) |

* *TSP-1 = previous version from 2014. TSP-1.2 = improved gas distribution implemented (developed in ForskEL project 2015-1-12276). TSP-1.3 = TSP-1.2 + new contact layer (oxy side).*

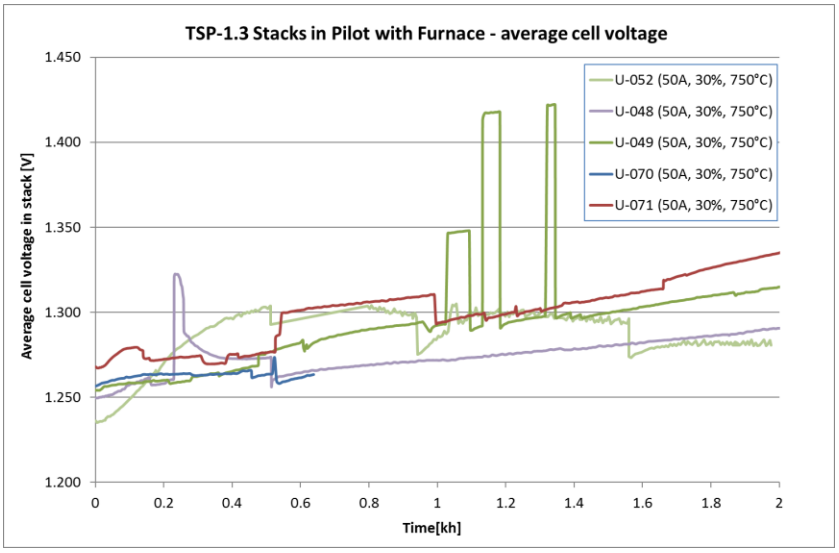


***Figure 26.*** *Stack tests conducted in M2.3 including one reference stack (U-052, TSP-1.3 with no modifications) from previous testing in ForskEL project 2015-1-12276 to compare different stack modifications. NB! The jumps in cell voltage are associated with periods with different operating profile, dynamic load and/or thermal cycles.*

Comparing the reference stack (U-052) with the stacks having different modifications to coatings and contacting, it is clear that the initial behavior during the first 1000h of testing is quite different. The reference stack (U-052) had a much higher initial degradation rate during the first 500h and then the average cell voltage levels out, actually with some activation until 2000h. Based on previous data we know that this activation is due to improved contacting on the air side with time. The stacks with modifications to coatings/contacting showed a more linear degradation profile from beginning of life (BOL). The average cell voltage in the modified stacks cross the reference stack at around 1000h. The modified stacks also start with a higher initial cell voltage compared with the reference stack. From this we concluded that the modifications to the coatings/contacting influence the BOL behavior as well as the degradation profile of the stacks. It would be desirable to have a low initial degradation, as was the case with the modified stacks, combined with a flattening of the degradation rate with time, similar to U-052. The learnings from testing the stacks were later used to make further iterations on certain stack modifications. These tests will be discussed in section 1.5.3.3 (M2.5). Worth noting is that U-71 was kept running and at project end it was still in operation with a total run time of >10000h (see section 1.5.3.3 (M2.5) for a comparison). The stack test results were furthermore used to validate the 3D multi-physics stack model, see more in section 1.5.4.3.

***M2.4: More than one year operation of a stack for syngas production demonstrated (KEY)***

In order to demonstrate proof-of-concept of long term operation of stacks in $CO_2$ electrolysis, one key milestone in the project was to show at least one year operation of one stack for CO production. To make the test most system relevant it was decided to test a SOEC Core at Haldor Topsoe's test facility. An SOEC Core is the module that will be installed in a system having all the required balance-of-plant components (heaters, heat exchangers etc) to make easy installation and maintenance possible. The only connections needed to the SOEC Core is power and gas. The experimental SOEC Core tested had two TSP-1 (version TSP-1.3) stacks installed (U-050 and U-051, similar to U-052 mentioned above) and the results from a >1 year test is shown in Figure 27.

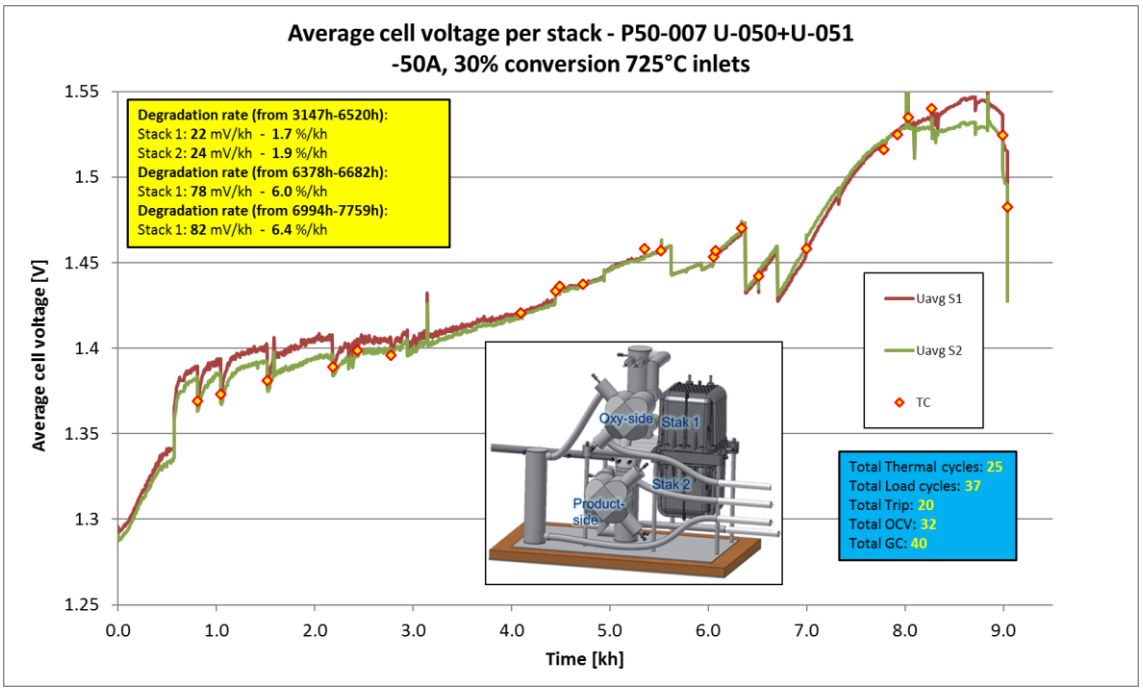


***Figure 27.*** *More than one year operation of a SOEC Core having two stacks (U-050 and U-051). The inset shows a schematic of the internal parts of the SOEC Core having two TSP-1 stacks in a "boxer mode" configuration.*

After a run-in period for approximately 500h the operating parameters were set to the conditions mentioned in Figure 27. The initial degradation profile during the run-in period resembles the behavior of the U-052 reference stack in Figure 26. Throughout the test the stacks and the SOEC Core experienced a number of events (25 thermal cycles, 37 load cycles, 20 trips etc). Some of the events resulted in increased degradation, especially when accidentally exposed to too high conversion, which leads to internal carbon formation. Too high conversion, due to partial loss of $CO_2$ flow, eventually caused fatal damage to the stacks, and the test was stopped just after reaching 9000h of operation. This in itself is an encouraging result. During the test it was decided to increase the inlet temperature, from the initial 725°C, in several steps. The intention was to investigate if increasing temperature, which results in lower overpotential on the electrodes, would mitigate the degradation. The temperature increase was done in steps from around 5800h (as seen in Figure 27 as sharp decrease in cell voltage). The increased temperature, however, increased the degradation of the stacks. Interestingly, when the stacks come closer to (or slightly above) the thermoneutral operation for $CO_2$ electrolysis (around 1.48 V) the cell voltages started to level out again. The fatal event at end-of-life was not caused by the stacks degrading as such, it was related to a system event. It is of course desirable to have stacks with long lifetime and high robustness. However, the tests also shows how critical it is to have safety controls in the system to avoid events similar to the ones the stacks were subjected to in this one-year test.

After this successful one-year SOEC Core test, Topsoe started other long-term SOEC Core tests (not part of this project, but reported in combination with other dissemination activities at SOFC-XVI in 2019). Based on the learning from this project, among other things the pilot control system has been improved, leading to less trips and unwanted shut-downs. These new stack test results are very promising, indicated by >7000h of operation of a SOEC Core (2 stacks) with <0.5% V/kh degradation during the last 6000h. These combined results are very encouraging for the future development and commercialization of Topsoe's SOEC technology.

#### 1.5.3.3 WP2.3: Improved stack design and operation for enhanced reliability and lifetime

Based on the results from previous sections, ideas for improving stack design was implemented and evaluated with the objective to improve reliability and lifetime.

***M2.5: Optimized cells with improved lifetime tested in stack with improved design – show potential for longer (2 year) lifetime (KEY)***

In section 1.5.3.2, a number of modifications to specific stack components were investigated, which gave valuable input to further development. Since it was not successful to develop improved cells in section 1.5.2.3, the development focus on stack level instead focused on the following areas/components, where significant progress was made during the project:

- *Improved contact solution on the fuel side of the cells.*
- *Improved coatings on the interconnect (with focus on the oxygen side).* The new experimental coating solution qualitatively results in improved contact on the air side with similar or improved corrosion properties compared to previous solution in TSP-1.
- *Decrease external leaks into the stack.* Improved quality control and minor modifications to sealing procedures of the stack resulted in less external leaks, measured as an increase in the open circuit voltage by >15 mV.

Two different stacks were first built (U-092 and U-096) to evaluate yet a number of different modifications (compared with data in M2.3). Based on the promising results from those initial tests, one final stack was built in the project having the most promising modifications and solutions in one single stack (U-115). Table 5 summarizes what components and procedures that were modified in the different stacks.

***Table 5.*** *Summary of stacks tested in $CO_2$ electrolysis to achieve M2.5. U-092 and U-096 had different combinations of stack component modifications in various cell groups, whereas U-115 had same modifications throughout the stack to evaluate the most promising solutions collectively.*

| Stack-ID: | Stack gen.* | Modification | Run time (h) |
|---|---|---|---|
| U-092 | TSP-1.3 | • Modification #1: new improved coatings on interconnects on both sides<br>• Modification #2: Similar to #1 but different coating on air side | 2000 |
| U-096 | TSP-1.3 | • Modification #2 as in U-092 and:<br>a) New contacting solution on fuel side<br>b) Improved sealing procedure<br>• Modification #3: Similar coating on fuel side interconnect as in #2, different coating on air side + a) and b) solutions | 1700 |
| U-115 | TSP-1.3X | • Modification #2 + a) and b) solutions in U-096 in whole stack | 2600 (testing cont.) |

* *See Table 4 for details.*

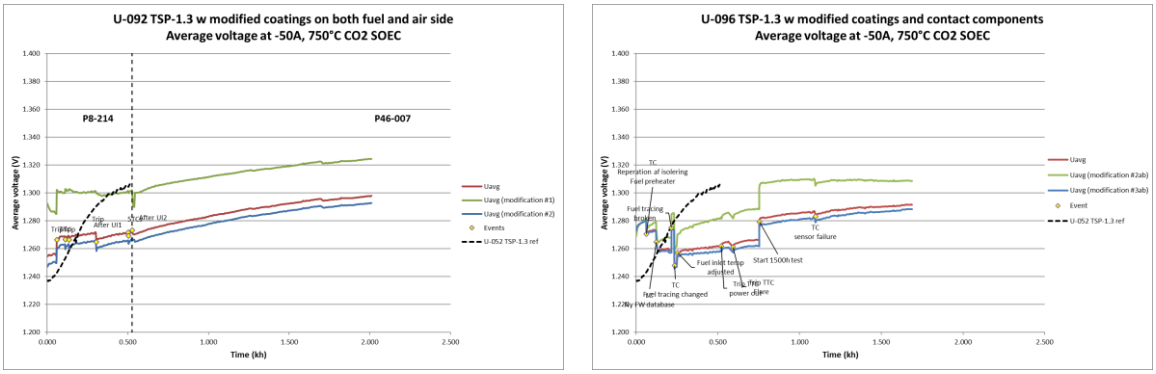


***Figure 28.*** *Stack tests of U-092 (left) and U-096 (right).*

Figure 28 shows the results from the 2000h testing of U-092 and U-096. There were a number of pilot related events during the first 1000h of operation of both stacks. However, there were clear indications that the initial degradation seen on previous stack generations (see U-052 in Figure 26) was again lower. Furthermore, the linear degradation in U-092 was <1% V/kh during the final 200h of testing. In U-096 the results were even more promising, especially for Modification #2ab (see Table 5). Here, there were no degradation during the last 500h of the test. It was therefore decided, as mentioned above, to test those solutions collectively in one single stack (U-115). Figure 29 shows the results from the still ongoing test of U-115. The initial degradation is very low and the total degradation from BOL is currently <0.7% V/kh. Furthermore, the voltage increase seems to level out similar to the same modification in U-096. Comparing U-071 (see Table 4), which has currently passed >10000h of operation, with the U-115 stack nicely illustrates the promising lifetime perspectives of U-115. Even though U-071 has a relatively high average cell voltage, there are currently no indications of stack failure from e.g. gas chromatography analysis (a useful in-line tool when evaluating cross-over leaks in operational stacks, which is a sign of potential severe stack damage). Looking at the trend for U-115 one can only speculate on the "lifetime" of the stack if allowing the same cell voltage as in U-071.

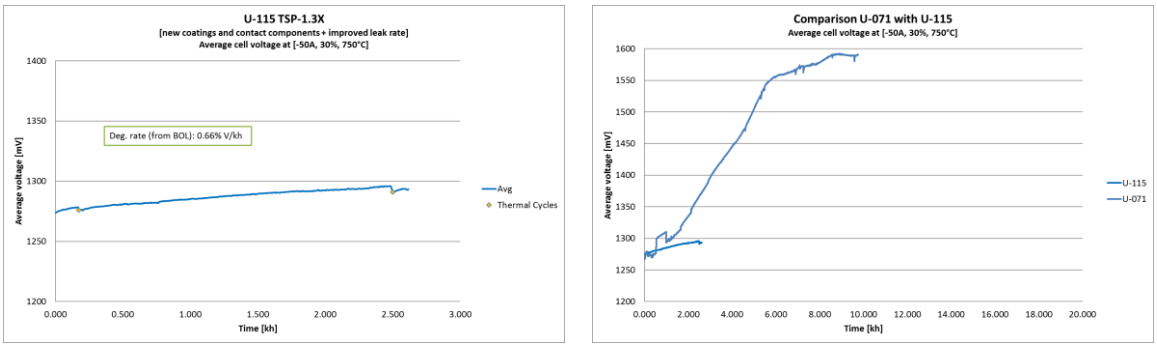


***Figure 29.*** *(Left) Stack test of U-115. (Right) comparison between U-115 and U-071 (operated for >10000h) at same operating conditions. NB! The x-axis has been extended to 20000h for illustrative purposes.*

Based on the results obtained from all the tests above there are strong indications that the lifetime of the TSP-1 (or more specifically TSP-1.3X) stack will be >2 years in $CO_2$ electrolysis. The stack will be kept in operation as long as possible, and hopefully demonstrate test data to show the anticipated long lifetime. Topsoe will continue evaluating the different modifications on component level and in production, and likely implement many of the promising modifications tested in U-115 in coming upgrades of the TSP-1 stack.

### *1.5.4 WP3: Optimized cells and stacks by advanced modelling*

The objective of this work package was to develop modelling tools to predict critical failure mechanisms in the SOC cells and stacks in order to reach a safe operation window for the stacks. The models was also used facilitate improved stack designs, which should increase

the safe operation window and ultimately improve the reliability and lifetime of the stacks (evaluated in WP2).

#### 1.5.4.1 WP3.1: Enhancement of 3D multi-physics model to simulate mechanical failures

Thermo-mechanical analysis of the entire SOEC stack at operational conditions are computationally challenging, if the geometry of metallic interconnects is considered explicitly. This is particularly the case when creep deformations in the interconnect are considered in addition to elasticity. In this work, this problem is addressed using homogenization, or so-called multiscale models, which tremendously minimizes the computational needs.

***M3.1: Model for homogenization of the creep and contact demonstrated and made available for investigations***

**Overall modelling concept**

When homogenization is used, the actual geometry is replaced by a homogeneous block of an "equivalent" material. Hereby the number of computational volumes (finite elements / control volumes) are heavily decreased and likewise is the computational effort. The challenge is however to find a mathematical description for the equivalent material, which can describe the combined response of the actual geometry and the actual material behavior.

**Modelling of the actual geometry and material behavior**

In the SOC stack the metallic interconnect is the component which will creep far the most, why this has had the focus in current work. The geometry modelled represents that in HTAS's SOC stack, i.e. corrugated shape, see Figure 30.

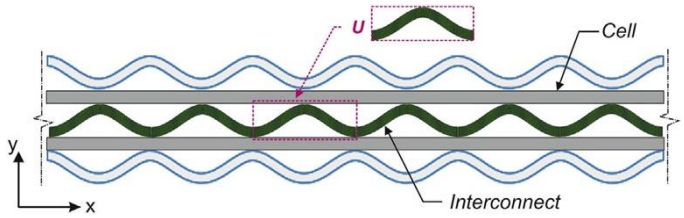


***Figure 30.*** *Sketch of cross-section of a SOC stack, with specification of the modelled repeating unit cell U.*

The interconnect steel, Crofer22APU, has previously been characterized and here both elastic and creep behaviors are included in the model. Furthermore, the mechanical contact from pressing the interconnect into the cell have been described in the models, i.e. an increasing contact area with the pressing, see Figure 31.

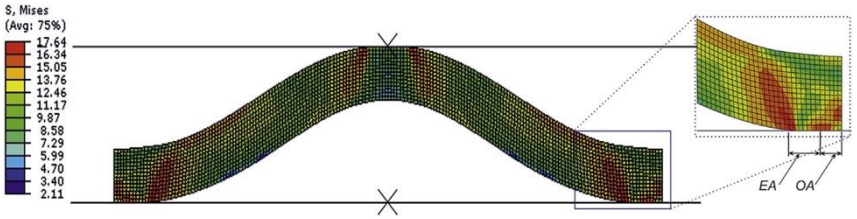


***Figure 31.*** *Distribution of von Mises stress in the repeating unit of the interconnect under vertical load, with a zoom on the contact area, which increases with the pressing (from 0A to also include EA) [1].*

The average deformation, $E_{yy}^{vp}$, of the unit cell over time from vertical pressing, varies for different load levels, $S_{yy}$, see Figure 32a. In Figure 32a, the variation of strain over time is initially curved, which is due to establishing of the contact. After some deformation the steady state creep results in a linear behavior over time. From Figure 32a it is also clear that

the creep rate is also non-linear itself (e.g. the slope of the 0.45 MPa line is not the half of that for the almost double as large load of 0.85 MPa).

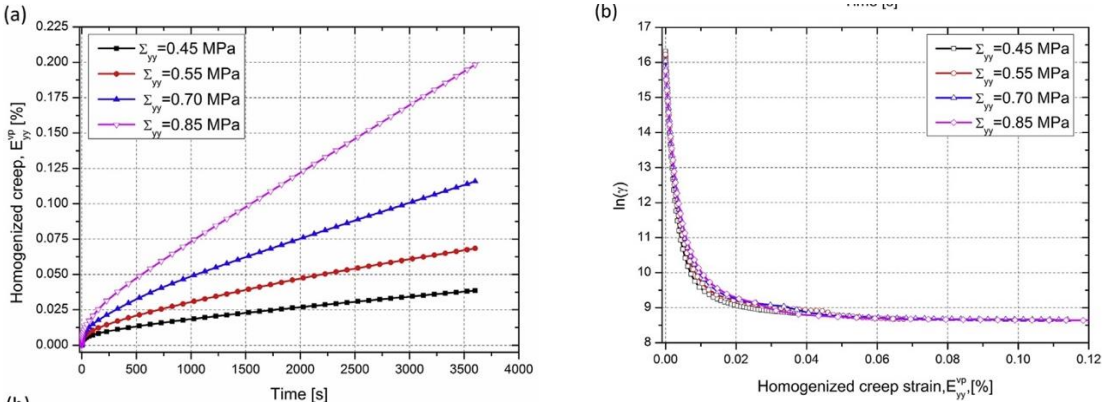


***Figure 32.*** *a) Creep strain $E_{yy}^{vp}$ over time for different vertical loads $S_{yy}$, and b) Normalization of creep strain in order to describe the contacting [1].*

**Modelling of the homogenized material**

When pressing the homogenized equivalent material, it should provide the same average response as the actual geometry and material, i.e. the same deformation as shown in Figure 32 for the same loads. To handle the non-linearities (creep and geometric) a new method for normalizing the creep and the contacting jointly was found, such that the combined response can be represented by a single equation, being:

$$\dot{\boldsymbol{E}} = \frac{3}{2} A^H \left( \frac{\boldsymbol{\Sigma}_{eq}}{G^H} \right)^{n-1} \frac{\mathbf{m}\boldsymbol{\Sigma}}{G^H} \circ \boldsymbol{\Gamma} \qquad (1)$$

where, $A^H$, $G^H$ and $n$, are creep parameters of the homogenized body, $\mathbf{m}$, is a square matrix consisting anisotropic coefficients, $\boldsymbol{\Sigma}'$ and $\boldsymbol{\Sigma}_{eq}$, are the average deviatoric and equivalent stresses, respectively. The vector $\boldsymbol{\Gamma}$ handles the non-linearity from contacting for different load directions [1].

**Demonstration using temperature profiles from HTAS stack models**

To integrate with the current SOC stack models at HTAS, the temperature variation was transferred from these models. The temperature distribution was simulated for co-flow and counter-flow for three different cases: Low current, Low conversion (LL), Medium current, Medium conversion (MM) and High current, High conversion (HH). Using the temperature profiles from these simulations the stress variation during operation for 10,000 hours and during shut-down was simulated. The maximum vertical stress over time, responsible for loss of contact between cell and interconnect, is shown in Figure 33.

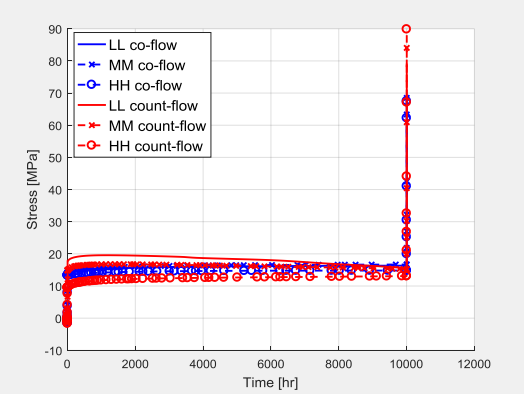


***Figure 33.*** *Maximum vertical stress in the stack during operation and shut down for the six cases described in the text.*

### 1.5.4.2 WP3.2: Development and implementation of 2D sub-model

Carbon deposition in the fuel electrode will result in irreversible damage. The current SOEC stack models describes the gas composition in the flow channels, but not at the most critical point locally below interconnect contact ribs. Therefore, the relationship between the channel gas compositions and the local gas compositions has been modelled at different current densities and gas compositions to obtain a "safety factor" to guide the stack operation.

***M3.2: 2D unit cell model finalized***

**Overall modelling concept**

The gas-channels through the stacks are relatively straight, and so is the channel defining array of contact ribs / points. All cross sections perpendicular to the flow direction are thus identical (where there is contacting), and transport perpendicular to the flow is thus well approximated by a 2D model. The transport below the contact points in the porous electrodes are dominated by diffusion, and convection can thus be neglected, simplifying the geometry to the one shown in Figure 34.

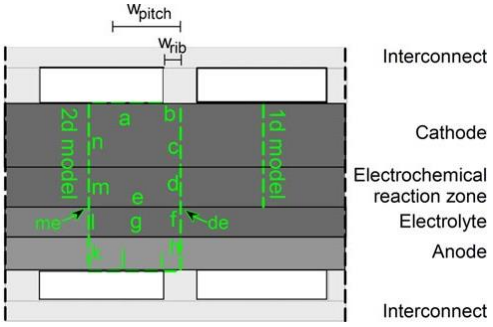


***Figure 34.*** *Sketch of the cross-section of cell and interconnect in an SOC stack, with the point "de" marking the critical point for carbon deposition [2].*

**Modelling of CO concentration at various current densities**

The gas composition in the electrodes depends on the gas-composition in the channel, distance from the channel, the current density, and the geometric parameters of the channel and rib ($w_{pitch}$, $w_{rib}$ in Figure 34). An example of the distribution of CO is show in Figure 35.

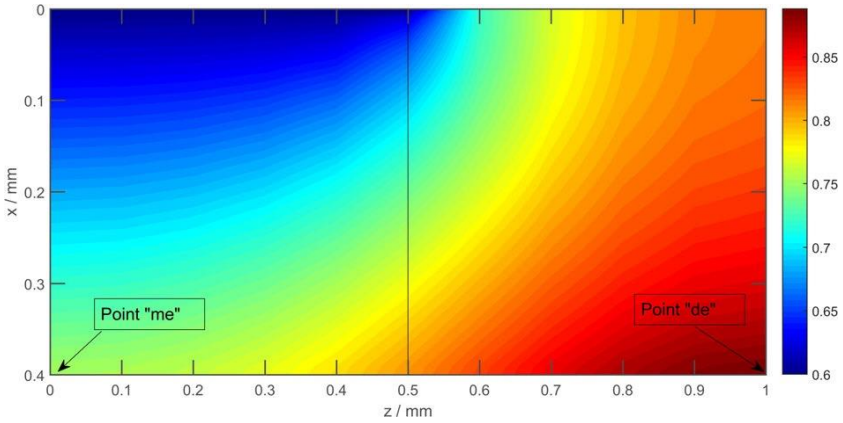


***Figure 35.*** *CO mole fraction in the fuel electrode at 700℃, 0.5 A.cm$^{-2}$, ε = 0.3, τ = 3, de = 400 µm, $x_{CO}$ = 0.6, $w_{pitch}$ = 1 mm and $w_{rib}$ = 0.5 mm [2].*

The model was used to simulate the conditions at various geometrical parameters, current densities and gas compositions at 750°C. The results are shown in Figure 36. As seen in Figure 36, the difference in CO mole fraction between the gas channel and the critical point below the rib (de) is linearly proportional to the current density. This can be used to establish a safety factor, as the carbon deposition is heavily dependent on the CO concentration (the so-called Bouduard reaction).

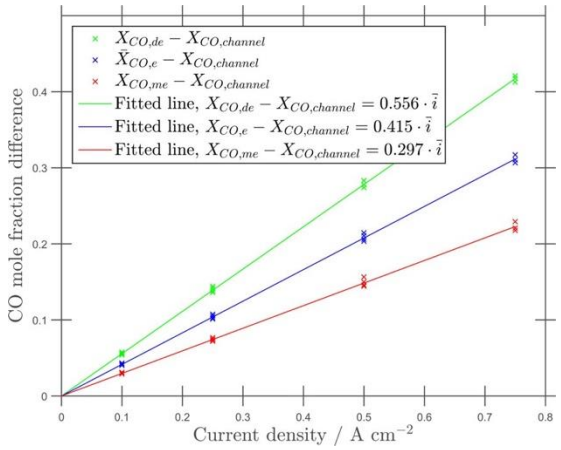


***Figure 36.*** *CO mole fractions difference between the channel and the point beneath the middle of the channel (point "me"), the point beneath the middle of the rib (point "de"), and the average mole fraction on boundary "e".*

#### 1.5.4.3 WP3.4: Predicting a window for safe stack operation

In this task the dependency of various stack operation parameters and other boundary conditions was investigated in order to determine a safe operation window for the SOEC stacks. This was done using the 3D multi-physics SOC stack model further improved in the project. The internal conditions and in particular the risk of detrimental carbon-deposition while operating an SOEC stack are crucial for safe operation. The operating parameters, such as the gas inlet temperatures, current, gas mixture, gas flow rate all influence the internal conditions, and if one is varied the influence of another is changed.

***M3.3: Window for safe stack operation modelled and analyzed***

**Overall modelling concept**

To investigate at which conditions operation can be performed without carbon deposition, the entire stack is modelled, while systematically varying these conditions. In the investigation following combinations are chosen: 5 different gas inlet temperatures, 3 different air flow rates, and 59 different combinations of flow and gas-compositions, yielding a total of 885 operating conditions. The entire stack is modelled using the homogenization approach for

mass transport (flow), electro-chemical reactions, heat transport, and charge transport (currents). Using this approach, the simulations were conducted on HTAS' cluster in less than a week. Using conventional models (not homogenized) and a conventional computer, this would have taken approximately 200 weeks (4 years) of simulation time [3].

**Modelling results**

Each stack simulation is thus a full 3D simulation, where all quantities simulated varies across the stack due to the non-uniform flow and temperature distributions and couplings between those and the electro-chemical reactions (temperature and specie dependent). An example of the output of such a simulation is found in Figure 37.

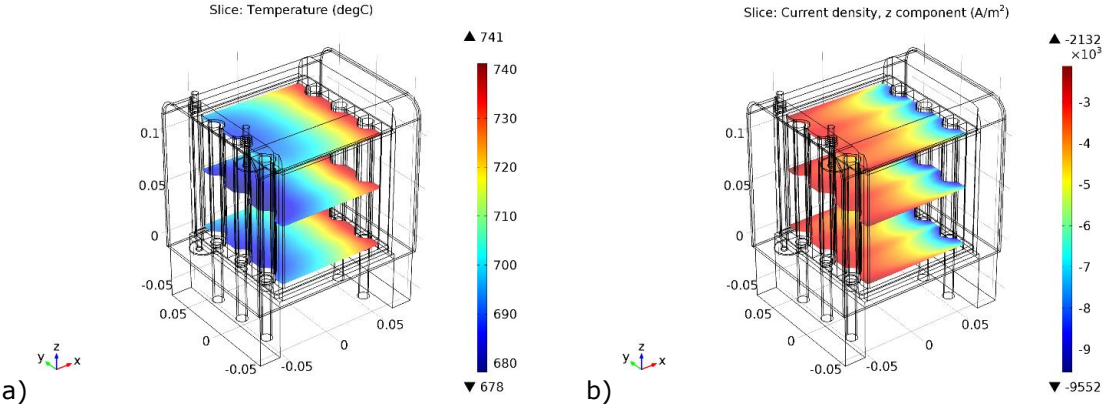


***Figure 37.*** *Examples of output from the 3D stack model; a) Temperature distribution, b) Current density distribution.*

From each of these simulations important information on the chance for failure, such as the most critical CO concentration and corresponding temperature is extracted. An example of the results from these hundreds of simulations can be found in Figure 38. Here it is shown that the outlet gas should contain no more than 29 % of CO if carbon deposition are to be avoided at lower currents, as the temperature margin otherwise becomes negative (for further explanation please refer to e.g. [2]).

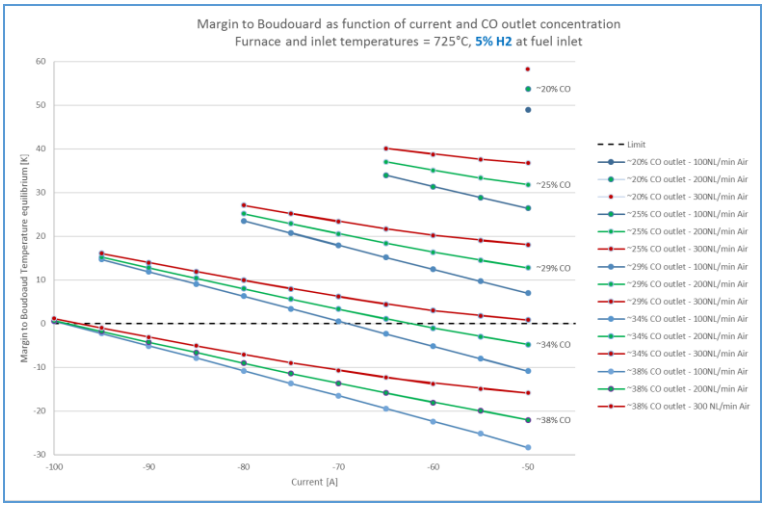


***Figure 38.*** *Temperature margin to carbon deposition at different currents*

A number of other important conclusions were drawn on these simulations; on the influence of adding hydrogen to the $CO_2$, on the influence of the furnace temperature, on the effect of changing the air flow rate, and on the relationship between the maximum local current density and total current.

### *1.5.5 WP4: Development of reversible and pressurized operation of SOECs*

The objective of this work package was to demonstrate pressurized and reversible operation of SOC stacks and investigate the impact of these operating conditions on the stack lifetime and performance. Another high risk objective was to demonstrate energy storage where hydrogen produced during electrolysis was to be stored and later used during fuel cell operation (in a virtual test bed thinking).

#### 1.5.5.1 WP4.1: Reversible operation – possibilities and limitations.

The promising results of a recent DTU Energy study [1] forms the basis for WP4.1. The study showed that reversible SOFC/SOEC operation on single-cell level can reduce the performance loss and mitigate certain degradation mechanisms, specifically related to adsorption of impurities and $O_2$ bubble formation at the interface between the positive electrode and the electrolyte. The objective of WP4.1 is to investigate if the effect translates to full-sized stack level.

The 75-cell TSP-1 stack used in WP2.1 has been used for WP 4.1 as well. The steam evaporator, which caused the failure after having successfully completed M2.1, was cleaned prior to the work presented below. Furthermore, the equipment was upgraded so that EIS could be measured with a current load, during the SOFC/SOEC cycling. A total of 4 cycles were completed over the course of ~175 h of testing and the results are summarized below.

***M4.1: Possibilities and limitations identified for extended SOEC stack lifetime using reversible operation***

**Initial characterization**

As described in WP 2.1, the stack was damaged by the incident with the steam evaporator. This is reflected in the initial OCV and voltage measured under a 25 A load, as seen in Figure 39. Up to ~80 mV lower OCV is measured, and especially RU60-75 appear severely damaged with up to ~500 mV loss with the current load. Although reversible operation has been shown to mitigate degradation, it was unlikely to revive the damaged cells, especially since the issues were likely linked to faulty sealing and/or delamination of RU components caused by the incident mentioned above. Nonetheless, the experiment was continued, since the stack still had seemingly well-functioning RUs.

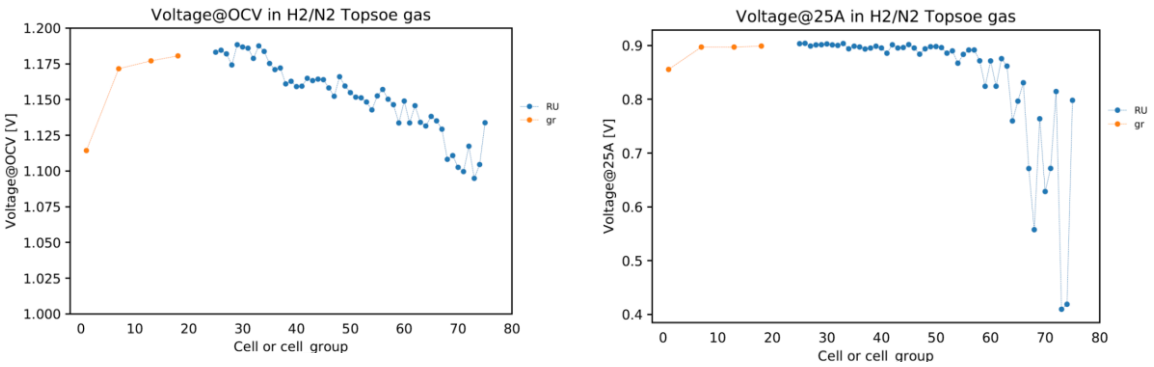


***Figure 39.*** *(Left) OCV during initial characterization. (Right) Voltage under 25A load during initial characterization.*

**SOFC/SOEC cycling**

The cycling between SOEC- and SOFC-mode was carried out at ~700 °C with a fuel gas of 90% $H_2O$ in $H_2$ and 20% $H_2O$ in $H_2$, respectively, and air to the oxygen electrode. The current load was 20A for both modes. As seen in Figure 40, the voltage spread was about 125 mV and 175 mV initially for SOEC- and SOFC-mode, respectively, and increased slightly for SOEC-mode during the experiment. Based on the voltage measurements, there does not appear to be any significant improvement in performance over the course of the 4 cycles. On the contrary, the voltage during SOEC-mode appears to increase slightly.

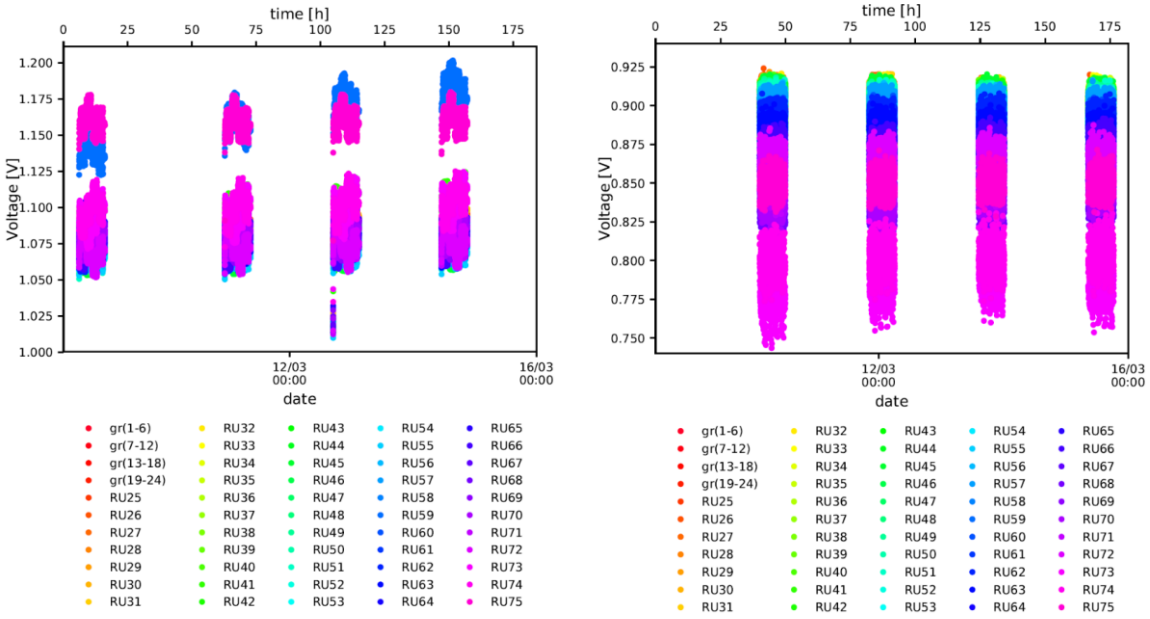


***Figure 40.*** *(Left) Voltage recorded during SOEC-mode for the 4 cycles. (Right) Voltage recorded during SOFC-mode for the 4 cycles.*

**Impedance measurements**

EIS were recorded during either mode, as quantified in Figure 41. Please note that the quantification is based on rather noisy data, so for instance the $R_P$ values of RU70-75 presented in Figure 41(D) are in fact much larger. Likewise, the apparent change in $R_S$ and $R_P$ during SOEC-mode for cycle 4 compared to the previous cycles, is simply due to noise.

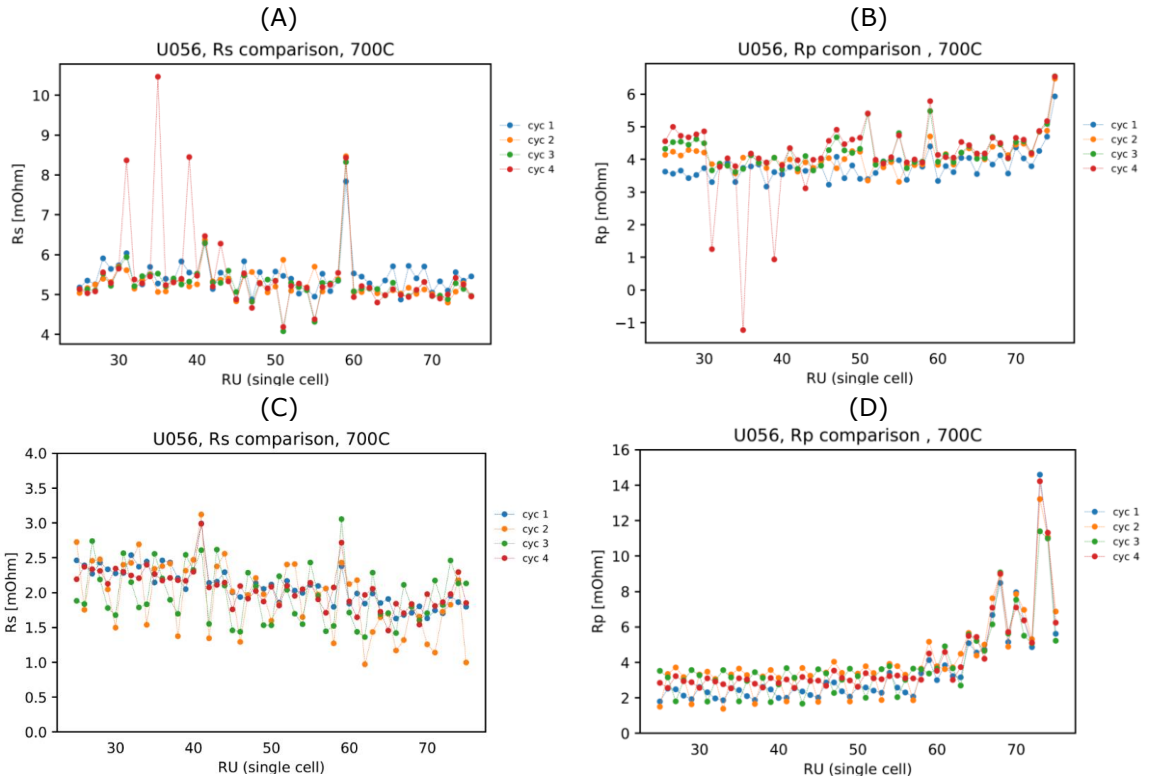


***Figure 41.*** *(A) $R_S$ measured on RUs during SOEC-mode for the 4 cycles. (B) $R_P$ measured on RUs during SOEC-mode for the 4 cycles. (C) $R_S$ measured on RUs during SOFC-mode for the 4 cycles. (D) $R_P$ measured on RUs during SOFC-mode for the 4 cycles.*

In general for both modes, there is no significant difference between cycle 1 and cycle 4, for both RS and RP. With the uncertainty of the damaged stack in mind, we conclude that the number of cycles was insufficient for assessing with certainty the beneficial effect of

reversible operation at stack level. The time period of each cycle should also be investigated in future work, as the optimization of this on single-cell level did enhance the effect.

#### 1.5.5.2 WP4.2: Pressurized SOEC operation

The objective of this work package was to improve the test facility for pressurized stack tests to handle larger and more technology relevant stacks from HTAS. The intention was to use the improved test facility to demonstrate pressurized steam and co-electrolysis operation on HTAS' TSP-1 stacks.

***M4.2: Technologically relevant HTAS stacks tested at elevated pressure***

**Initial pressurized testing**

To prepare the pressure vessel and rig for the larger TSP-1 stack from HTAS, a test of a smaller 30-cell SOFCMAN 301 stack was completed. The simple schematic shown in Figure 42 illustrates the pressurized rig design, which would later be used for testing the TSP-1 stack as well. The small-stack test was successfully carried out with carbonaceous gases at 18.7 bar and internal methanation in the stack was shown.

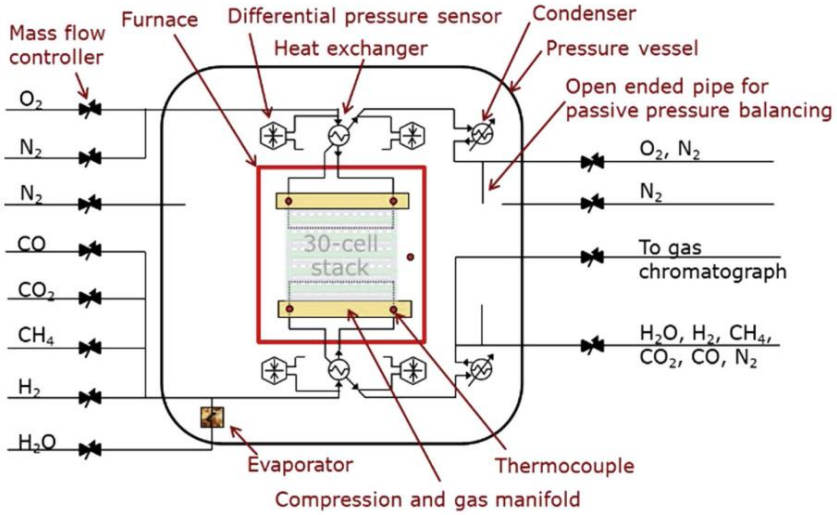


***Figure 42.*** *The setup used for testing at elevated pressure.*

The stack consisted of 30 cells with 63 $cm^2$ footprint and similar cell types as those tested in other parts of the project. After NiO reduction at elevated temperature, the pressure was increased in four steps while flowing a mixture of $H_2$ and $H_2O$. EIS and iV spectra were recorded at each step, as shown in Figure 43.

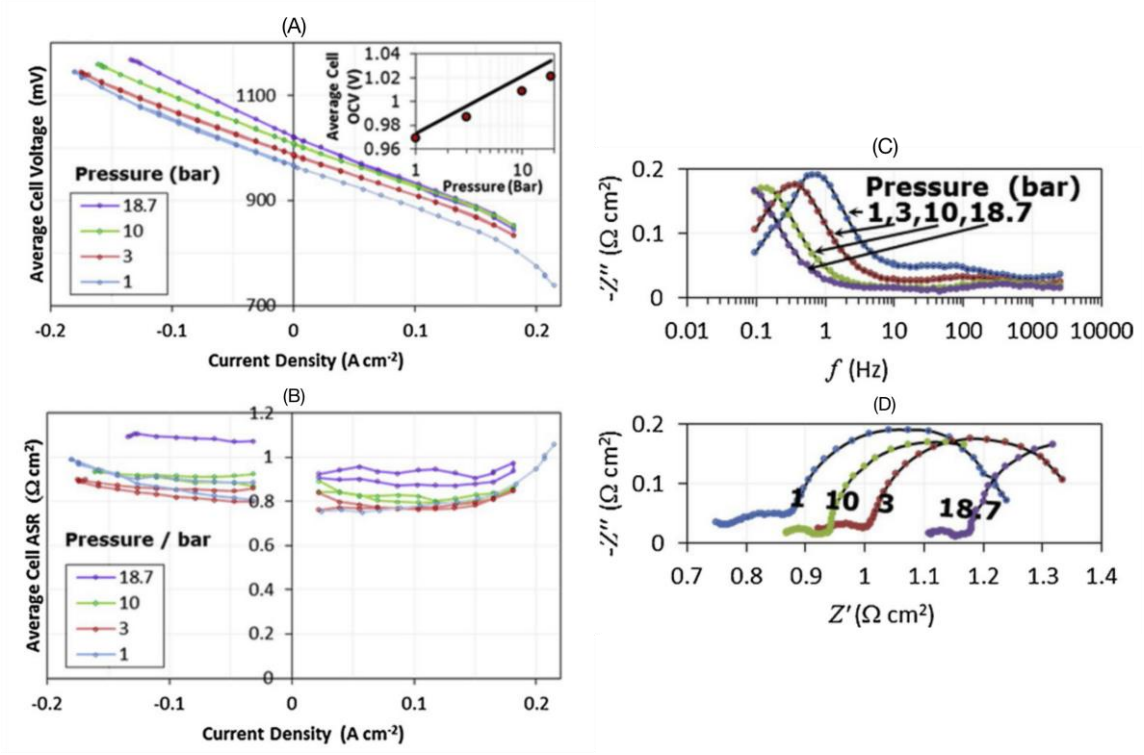


***Figure 43.*** *iV and EIS measurements at pressures up to 18.7 bar. (A) iV, where the inset shows the theoretical OCV (line) vs. recorded OCV. (B) Average cell resistance at elevated pressure. (C) Bode plot showing a decreasing peak frequency for the conversion arc. (D) Nyquist plot showing a somewhat fluctuating ohmic resistance.*

Next, carbonaceous gases was fed to the stack and via gas chromatograph it was shown that the stack produced methane, increasing the content from 0.22 vol% to 18 vol%. It was also discovered that the stack was leaking internally.

Lastly, degradation of the stack was investigated at a pressure of 18.7 bar. The rate of degradation resembled that of operation at atmospheric pressure. Post-mortem SEM revealed several degradation mechanisms occurring, i.e. contact loss between cell and interconnect, cracks in the oxygen electrode and electrolyte, delamination between fuel electrode and electrolyte, and fuel electrode oxidation.

For details and further discussion of the results, please see Jensen et al (section 1.5.7., peer-reviewed publications [7])

**Experimental setup for TSP1 testing**

The setup with integrated heat exchanger and preheater dedicated for the TSP-1 high-pressure stack testing was developed at DTU Energy. Figure 44 shows the integrated stack holder with heat exchanger and pre-heater on the left, and on the right the unit after being lowered into the pressure vessel is shown.

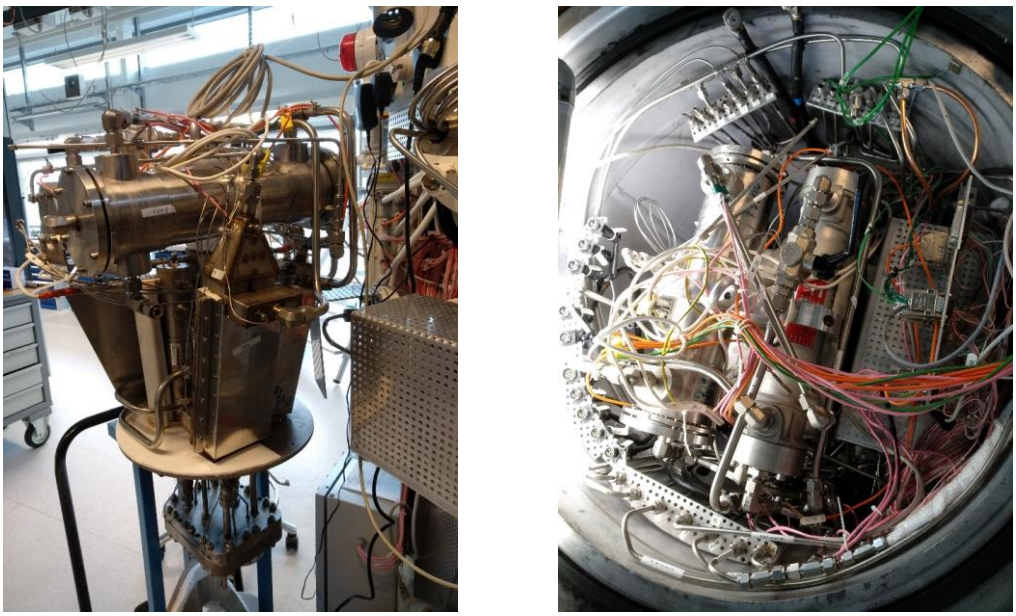

***Figure 44.*** *Experimental setup developed for pressurized testing of HTAS TSP-1 stacks.*

**Results**

Before heating up, the stack was pressurized to 3 bar with 500 L/h $N_2$ supplied to the fuel electrode and 500 L/h air supplied to the oxygen electrode. For heating up at 3 bar, gas to the fuel electrode was changed to 500 L/h of 5% $H_2$ in $N_2$, and the stack was heated to 650°C with a 1°C/min ramp-rate. As shown in Figure 45, the voltages of the 13 cells group look reasonable in the beginning (initial 3 hours). However, cell group 12 starts to drop in voltage after 4 hours at 650 ˚C, which caused further voltage-drops on the neighboring groups. After analyzing the data in greater detail, e.g. gas flows, gas composition, temperatures, or the differential pressure of each electrode compartment (Figure 45, bottom), there is no clear cause of the observed voltage drops. Nevertheless, the other cell groups appeared to survive and it was decided that the pressurized test would continue to obtain iV curves and test the lifetime of the stack.

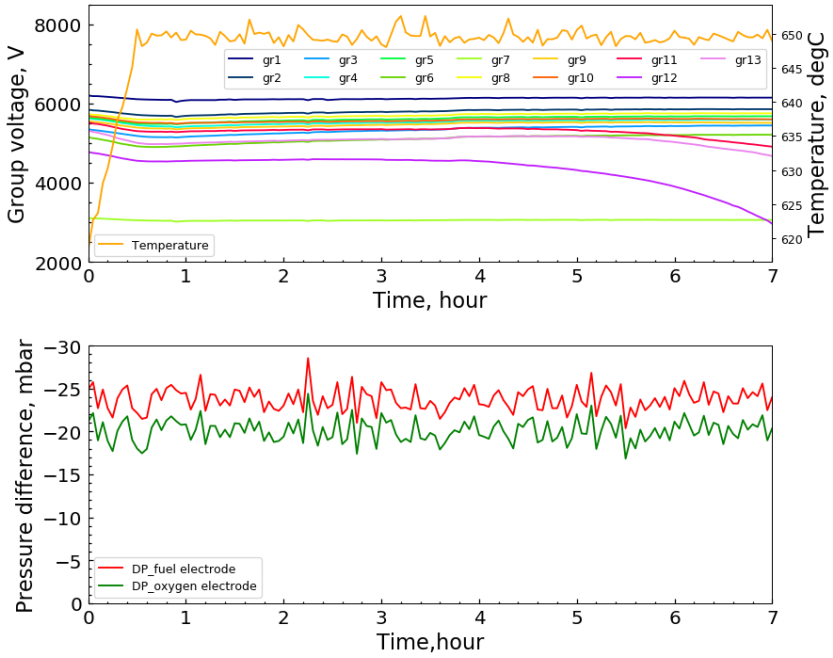


***Figure 45.*** *Cell group voltages and electrode differential pressure during heat up.*

Figure 46 show the iV characterizations of cell group 1 at 3, 5 and 8 bar at 725 ˚C with 80% $H_2O$ + 20% $H_2$ supplied to the fuel electrode and air supplied to the oxygen electrode. The voltage increases with pressure as expected according to the Nernst equation. Performance

at 5 bar and 8 bar is similar, and considerably worse than at 3 bar. This may be due to an increasing OCV and significant degradation caused by the damaged neighboring cell groups.

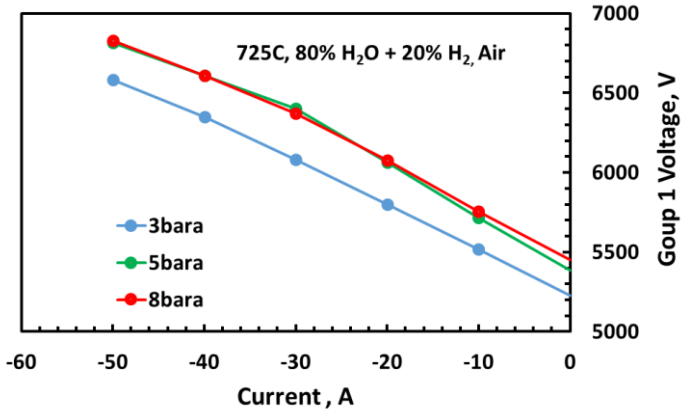


***Figure 46.*** *iV characterization at 3, 5 and 8 bar at 725 °C with 80% $H_2O$ + 20% $H_2$ to the fuel electrode and air to the oxygen electrode.*

A brief period of constant current operation was conducted with 25 A, as presented in Figure 47. The test was cut short after 80 hours of operation due to a severe gas leak in the stack. During operation the stack appeared to activate, but it is also worth noting that the decreasing voltage may also be affected by leak occurring in neighboring cell groups.

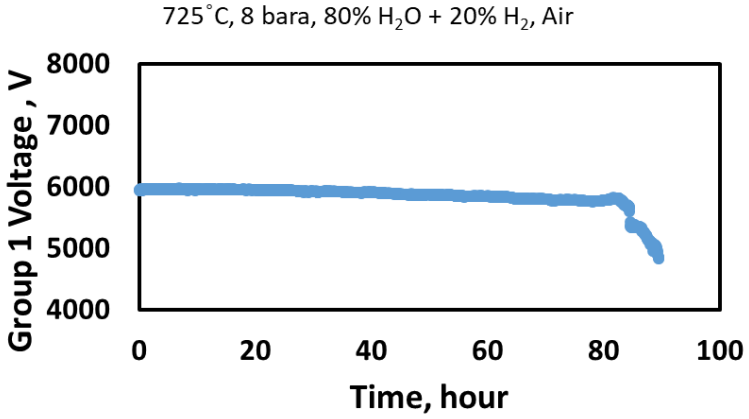


***Figure 47.*** *Group 1 voltage evolution as function of operation time*

In conclusion, the milestone is considered partially fulfilled. Pressurized testing is extremely complicated to carry out with many potential causes of malfunction. However, the collaboration between HTAS and DTU on this novel aspect of the SOEC technology will continue in future projects.

#### 1.5.5.3 WP4.3 Pressurized reversible systems and electricity storage demonstrated

It was initially planned to combine the results from WP4.1 (reversible operation) and WP4.2 (pressurized operation), and furthermore store the produced electricity from the reversible operation.

***M4.3: Electricity storage based on dynamic pressurized reversible operation of SOCs demonstrated (KEY)***

As several issues complicated the pressurized tests, as described in the preceding sections, WP4.3 was not initiated in time and completion of M4.3 was not reached.

### *1.5.6 WP5: Analyzing market opportunities and demonstration of system components*

The objectives of this work package were to 1) analyze and conduct a market study for small-scale off-grid power systems requiring extended storage time, 2) identify the most promising markets for small-scale on-site syngas production and 3) commercial demonstrations of key technology components

#### 1.5.6.1 WP5.1: Analyses of off-grid power systems with extended storage time

***CM1: Report on market analysis of off-grid power systems requiring extended storage time***

Faced with the awareness of the rapid increase of climate changes in recent years combined with falling prices on solar energy, the demand for sustainable storage solutions for solar energy has never been greater. The market for all storage solutions is growing rapidly and most of the technologies today are based on battery technology that have limitations on charging speed and capacity. The hydrogen storage solution does not have this limitation as the storage is an external unit, which can be easily increased. All storage solutions will likely be used, depending on the application and willingness to pay a higher price for the storage, which will help new technologies to mature to be competitive.

Danish Solar Energy finalized a report to fulfill the CM1 milestone. The key points in the report are: 1) Off-grid power system is becoming a broader concept. 2) When looking upstream in the electricity power industry, transmission and distribution, we see a huge, untapped market, i.e. grid-scale energy storage. Energy storage will play a key role help to establish smarter, more flexible grids in many ways. 3) There is no doubt that a huge potential market for energy storage lie ahead, the key factor is if it is economically viable. Scale production and lower cost is the direction for product developers and manufacturers to pursue. 4) Evaluation of the cost or value of battery storage through lifetime.

In their market analysis, Danish Solar Energy (DSOL) also wanted to better illustrate the hourly solar energy yield from specific solar power systems. Data from the solar panels installed at DSOL are illustrated in Figure 48. Similar illustrations are intended to be used to better forecast the produced energy from a solar power system, and combine it with anticipated energy use and thus give input to potential demand for energy storage solutions and capacity.

| Lat 54,47<br>Lon 11,36 | Jan | Feb | Mar | Apr | May | Jun | Jul | Aug | Sep | Oct | Nov | Dec |
|---|---|---|---|---|---|---|---|---|---|---|---|---|
| 0300 GMT | 0,00 kWh | 0,00 kWh | 0,00 kWh | 0,00 kWh | 0,00 kWh | 0,01 kWh | 0,00 kWh | 0,00 kWh | 0,00 kWh | 0,00 kWh | 0,00 kWh | 0,00 kWh |
| 0400 GMT | 0,00 kWh | 0,00 kWh | 0,00 kWh | 0,00 kWh | 0,05 kWh | 0,07 kWh | 0,06 kWh | 0,00 kWh | 0,00 kWh | 0,00 kWh | 0,00 kWh | 0,00 kWh |
| 0500 GMT | 0,00 kWh | 0,00 kWh | 0,00 kWh | 0,06 kWh | 0,13 kWh | 0,14 kWh | 0,13 kWh | 0,09 kWh | 0,01 kWh | 0,00 kWh | 0,00 kWh | 0,00 kWh |
| 0600 GMT | 0,00 kWh | 0,00 kWh | 0,05 kWh | 0,16 kWh | 0,22 kWh | 0,21 kWh | 0,20 kWh | 0,17 kWh | 0,10 kWh | 0,02 kWh | 0,00 kWh | 0,00 kWh |
| 0700 GMT | 0,00 kWh | 0,00 kWh | 0,05 kWh | 0,16 kWh | 0,22 kWh | 0,21 kWh | 0,20 kWh | 0,17 kWh | 0,10 kWh | 0,02 kWh | 0,00 kWh | 0,00 kWh |
| 0800 GMT | 0,04 kWh | 0,13 kWh | 0,24 kWh | 0,34 kWh | 0,38 kWh | 0,34 kWh | 0,35 kWh | 0,35 kWh | 0,27 kWh | 0,20 kWh | 0,10 kWh | 0,04 kWh |
| 0900 GMT | 0,12 kWh | 0,21 kWh | 0,32 kWh | 0,41 kWh | 0,45 kWh | 0,41 kWh | 0,42 kWh | 0,42 kWh | 0,34 kWh | 0,26 kWh | 0,17 kWh | 0,12 kWh |
| 1000 GMT | 0,18 kWh | 0,27 kWh | 0,38 kWh | 0,47 kWh | 0,50 kWh | 0,45 kWh | 0,47 kWh | 0,47 kWh | 0,39 kWh | 0,31 kWh | 0,21 kWh | 0,17 kWh |
| 1100 GMT | 0,21 kWh | 0,30 kWh | 0,41 kWh | 0,49 kWh | 0,53 kWh | 0,48 kWh | 0,50 kWh | 0,50 kWh | 0,41 kWh | 0,32 kWh | 0,23 kWh | 0,19 kWh |
| 1200 GMT | 0,21 kWh | 0,30 kWh | 0,40 kWh | 0,48 kWh | 0,51 kWh | 0,47 kWh | 0,50 kWh | 0,49 kWh | 0,40 kWh | 0,31 kWh | 0,21 kWh | 0,17 kWh |
| 1300 GMT | 0,17 kWh | 0,27 kWh | 0,37 kWh | 0,44 kWh | 0,47 kWh | 0,43 kWh | 0,46 kWh | 0,45 kWh | 0,36 kWh | 0,26 kWh | 0,17 kWh | 0,13 kWh |
| 1400 GMT | 0,11 kWh | 0,21 kWh | 0,31 kWh | 0,38 kWh | 0,41 kWh | 0,38 kWh | 0,40 kWh | 0,39 kWh | 0,30 kWh | 0,20 kWh | 0,10 kWh | 0,06 kWh |
| 1500 GMT | 0,03 kWh | 0,13 kWh | 0,22 kWh | 0,29 kWh | 0,33 kWh | 0,31 kWh | 0,33 kWh | 0,31 kWh | 0,22 kWh | 0,11 kWh | 0,01 kWh | 0,00 kWh |
| 1600 GMT | 0,00 kWh | 0,03 kWh | 0,13 kWh | 0,20 kWh | 0,25 kWh | 0,24 kWh | 0,25 kWh | 0,23 kWh | 0,13 kWh | 0,02 kWh | 0,00 kWh | 0,00 kWh |
| 1700 GMT | 0,00 kWh | 0,00 kWh | 0,02 kWh | 0,11 kWh | 0,16 kWh | 0,17 kWh | 0,18 kWh | 0,14 kWh | 0,04 kWh | 0,00 kWh | 0,00 kWh | 0,00 kWh |
| 1800 GMT | 0,00 kWh | 0,00 kWh | 0,00 kWh | 0,02 kWh | 0,08 kWh | 0,10 kWh | 0,10 kWh | 0,05 kWh | 0,00 kWh | 0,00 kWh | 0,00 kWh | 0,00 kWh |
| 1900 GMT | 0,00 kWh | 0,00 kWh | 0,00 kWh | 0,00 kWh | 0,01 kWh | 0,04 kWh | 0,03 kWh | 0,00 kWh | 0,00 kWh | 0,00 kWh | 0,00 kWh | 0,00 kWh |

***Figure 48.*** *Illustrative table showing the hourly solar energy yield in kWh from a specific solar energy system in Denmark.*

DSOL also analyzed the energy consumption for a standard household in Denmark. A typical family in Denmark uses on average 5200 kWh/year[1]. Having an energy storage system capacity of 7 kWh one would be able to move e.g. the solar energy produced during the day and be able to cover the standby night load.

### 1.5.6.2 WP5.2: Demonstration of power electronics systems optimized for SOEC/SOFC-based off-grid power storage systems

***M5.1: Demonstration of power electronics systems optimized for SOEC/SOFC-based off-grid power storage systems***

An off-grid power back-up system will typically contain a number of electrical units operating at different voltage and current levels, e.g (DC) solar panels, (AC) generators, (DC) SOEC/SOFC unit and numerous pieces of AC and DC electrical application equipment. As power converters are relatively expensive it is critical to consider the optimum electrical interface design for such a system.

DSOL has developed and demonstrated their power electronics system – the "SMART controller" – and are able to control the output of multiple energy sources to potentially produce hydrogen from electrolysis or produce electric power. The system can optimize the competiveness of hydrogen storage, by analyzing the market potential and controlling the processes (see illustrations in Figure 49).

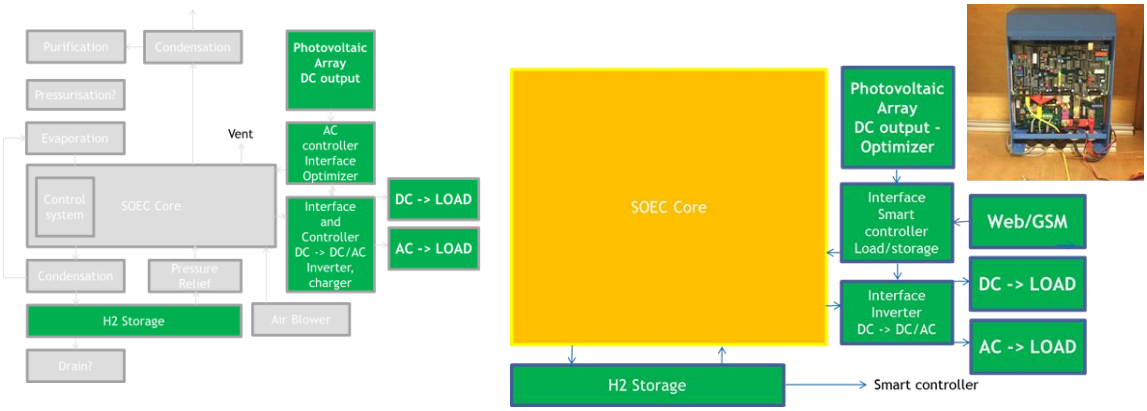


***Figure 49.*** *(Left) schematic illustration of a PV-SOEC/SOFC system used for developing the SMART controller. (Right) Illustration and picture of the SMART controller developed.*

The demonstration set-up at DSOL comprises the PV-array (32 modules of 250 Wp – total 8 kWp), a Fronius grid-connected inverter with communication tools and software, the SMART controller (developed in this project), and a "simulated hydrogen storage" using batteries. There are also hybrid controllers, which administrate and optimize the energy storage. For building and programming the SMART controller (Figure 49 (Right)) the following input and output were considered. The input can either be:

- Solar power
- The grid
- Wind power
- Other power generator

The output from the SMART controller was designed to be:

- Solar power direct to load or to store (as hydrogen via electrolysis)
- Hydrogen to load (via fuel cell operation) or sell to the grid
- Grid direct to load or to produce hydrogen (via electrolysis)
- Other generator to load or to produce hydrogen (via electrolysis)

### 1.5.6.3 WP5.3: Demonstration of small-scale low-cost hydrogen storage

[1] From https://sparenergi.dk/forbruger/el/dit-elforbrug (May 2019).

***M5.2: Small-scale low-cost hydrogen storage concept demonstrated (KEY)***

Hydrogen is the lightest gas in the world, which makes the gas difficult to store. There are several different methods to store hydrogen:

- By storing the hydrogen gas in liquid form
- By storing hydrogen as a gas in pressure vessels
- By storing the hydrogen in various types of metal powders.

As opposed to traditional gas storage, which typically requires a gas pressure exceeding several hundred bars, small-scale systems would benefit from low-pressure gas storage in the range 5-25 bar. As we only want to store the hydrogen for a relatively short time, 4-5 hours per day, mostly moving energy from day to evening/night, we do not need to store so much hydrogen, and we would then keep it at relatively low pressure (e.g. 5-20 bar). This makes it possible to use less expensive storage solutions such as traditional natural gas pipes.

Since the pressurized operation in WP4 was not successfully completed and the matureness of SOEC/SOFC reversible systems is not at a level where demonstration of the concept of storing hydrogen in natural gas pipes makes sense, we were not able to demonstrate the concept in reality. However, storing hydrogen in the natural gas grid (by adding more $H_2$ to the natural gas) or by simply using natural gas pipes for storage of hydrogen for shorter periods might still be a promising route for low-cost hydrogen storage in the future.[2]

### 1.5.6.4 WP5.4: Analyses of field testing data from small-scale syngas production unit

Prior to the Maturing SOEC project, HTAS sold the first commercial demonstration unit for small-scale CO production from electrolysis of $CO_2$. This demonstration unit was installed at the customer site (Gas Innovations, La Porte, Texas, USA) in Q1 2016. The purpose of this work package was to evaluate the operation of this demonstration unit, and based on the experience, refine HTAS' strategy for this specific niche market and how to reach larger (niche) markets.

***CM2: Analysis of field test data from small-scale syngas production unit – how to reach the next market***

A confidential milestone report was compiled, and certain specific details will thus not be shared in this report. This section will only summarize selected parts of the milestone report.

**What is eCOs™?**

Haldor Topsoe is commercializing a system for on-site CO generation based on solid oxide electrolysis cell (SOEC) technology (eCOs™). The system significantly reduces safety risks associated with handling and transportation of carbon monoxide, as CO can be produced on-site and on-demand from unhazardous $CO_2$ feedstock. The standard eCOs™ Plant is capable of supplying between 10 and >100 $Nm^3$ CO at 99.0% purity, but can also be customized to produce CO at 99.999% purity.[3]

An eCOs™ Plant is a stand-alone unit with power, $CO_2$, and product gas connections that allows the customer to produce carbon monoxide on-site and on-demand from carbon dioxide feedstock. A simplified schematic of the system is shown in Figure 50. During operation, carbon dioxide is fed to the fuel-side of the SOEC stacks, where $CO_2$ is converted electrochemically into CO using power from the grid. On the air-side of the SOEC stack, one molecule of $O_2$ is formed for every two $CO_2$ molecules that are converted into CO on the fuel-side. The CO-rich product gas is purified further using a patented process, resulting in a product stream of pure CO (>99% CO). The CO-depleted effluent stream from the gas

[2] H. Iskov, S. Kneck, Using the natural gas network for transporting hydrogen – ten years of experience, International Gas Union Research Conference 2017 Proceedings, IBP1057_17 (2017). https://www.dgc.dk/sites/default/files/filer/publikationer/C1703_IGRC2017_iskov.pdf

[3] See dedicated landing page for eCOs™ on Haldor Topsoe's website: https://info.topsoe.com/ecos

purification system is recycled and mixed into the $CO_2$ feed. The system can be modified to supply ultra-high purity CO (up to 99.999% assay) with $CO_2$ as the main impurity.

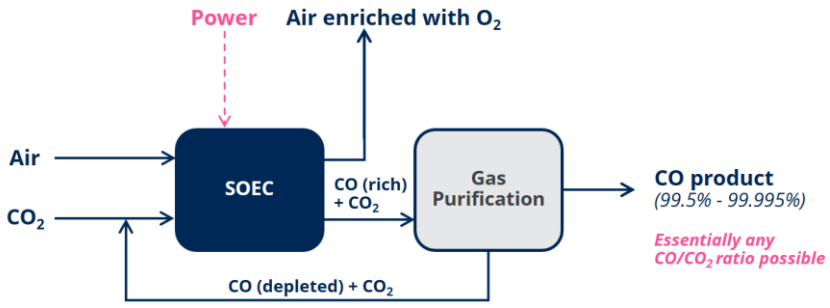


***Figure 50.*** *A simplified schematic of eCOs™ Plant.*

On-site CO generation using the eCOs™ technology has several important advantages compared to common alternatives, such as CO supply by tube-trailers or gas cylinders. First, CO is produced on-site from unhazardous $CO_2$ feedstock, which is safe to store and handle. Secondly, CO can be produced on-demand only when needed, reducing or eliminating the need for storing large amounts of CO on-site. This significantly reduces the safety risks associated with handling and transporting carbon monoxide. Thirdly, there is no inertia in the system, as CO production can be stopped instantaneously by cutting off the supply of power to the SOEC unit. An eCOs™ plant provides the customers with intimate control over their CO production, ensures security of supply, and drastically reduces costs for storage, rentals and connections.

**Operation of eCOs™ demonstration unit**

A demonstration eCOs™ Plant was supplied to Gas Innovations Inc. in January 2016 and is located in La Porte, near Houston, Texas, USA (Figure 51). The unit is compactly housed in a standard ISO 20-ft maritime container and functions as a turn-key fully automated CO production plant. The system is operated by Gas Innovations, and has demonstrated stable CO production at a capacity of 3-5 $Nm^3/h$ and 99.95+% purity.

***Figure 51.*** *Demonstration unit at Gas Innovations site at La Porte, Texas.*

Example gas analysis data from the demonstration unit, measured by Gas Innovations, are shown in Table 6.

***Table 6.*** *Example Certificate of Analysis of product from the eCOs™ demonstration plant. THC stands for total hydrocarbons.*

| CO (%) | Ar (ppmv) | $H_2$ (ppmv) | $N_2$ (ppmv) | $O_2$ (ppmv) | THC (ppmv) | $CO_2$ (ppmv) | $H_2O$ (ppmv) |
|---|---|---|---|---|---|---|---|
| 99.96 | 6 | 1 | 26 | < 0.1 | < 0.1 | 330 | < 2 |

Compared to traditional reformer-based carbon monoxide, CO produced using the eCOs™ technology has an inherently low content of hydrocarbons (mainly $CH_4$), $O_2$, $H_2$, and $H_2O$, which provides distinct advantages in a number of specialty and high-purity applications. Even higher gas purities (< 50 ppm $CO_2$ in product) have been achieved in the demonstration unit by fine-tuning the plant operation parameters. Figure 52 shows the

performance of two stacks operating in the demonstration plant over a 120-hour period. The stacks deliver a stable nominal output of CO gas.

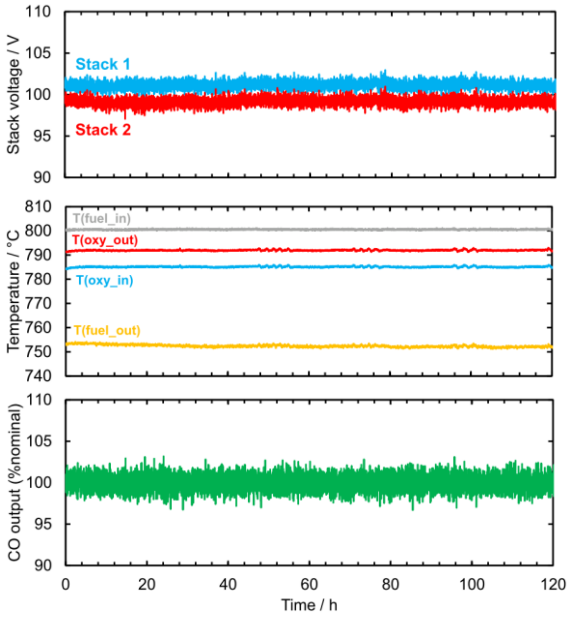


***Figure 52.*** *Example data from two stacks of the demonstration plant in La Porte, TX. Top: stack voltage for each stack. Middle: local temperatures in Stack 1. Bottom: CO production from the system (100% corresponds to the set point CO production value).*

**Strategic considerations for reaching future markets for SOEC-based systems**

Haldor Topsoe considers electrolysis an enabling technology for de-coupling the production of industrial chemicals from the use of fossil fuels and $CO_2$ emissions. In a world where greenhouse gas emissions from the chemical industry are under increasing scrutiny, alternative, less $CO_2$-intensive production methods for common chemicals are gaining traction. In such a context, electrolysis technologies, and SOEC in particular, can play a crucial role: when combined with renewable energy sources, electrolysis systems are able to carry out chemical conversions without carbon emissions.

However, the future is not here yet. The cost of using the SOEC technology (or any other available electrolysis technology) for producing hydrogen is still significantly higher than the cost of producing hydrogen from fossil fuels. Topsoe is convinced that catalysis will play a crucial role in solving the energy challenges we all face. Whether the future energy carrier of choice will be hydrogen remains to be seen. It could just as well be methanol, ammonia, or a combination of all. Which solution turns out to be right one will depend on the environmental footprint, how easy it is to store and use, security of supply, and many more factors, including the very important issue of cost.

The conclusion from the market analysis is that we need to continue using a stepping stone approach in order to reach the future larger markets. We need to bridge the gap between our current eCOs™ solution and a technical solution in the future (beyond 2030), where the vision and ambition is that SOEC will be the cheapest and preferred $H_2$ and CO production method, with large capacity, low cost and large scale production. The stepping stone approach means that we are looking for applications that contribute to a continuous increase in our electrolysis production capacity and hence lower the cost. A competitive advantage must also be present from the start, both for Topsoe as technology provider and for the potential customer and/or end-user. The stepping stone approach is summarized in Figure 53 below.

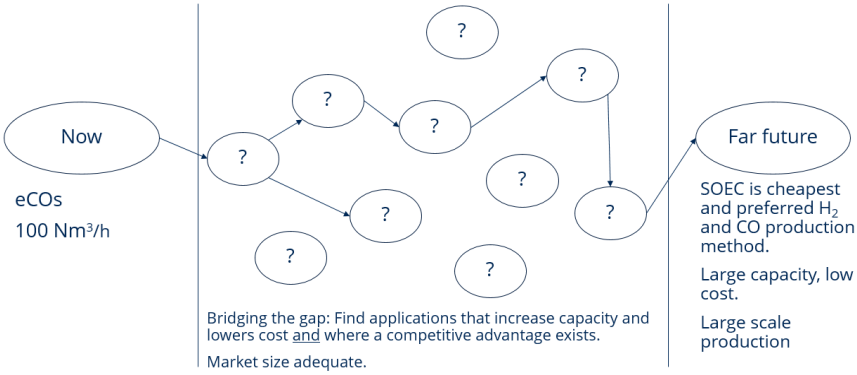


***Figure 53.*** *Schematic illustration showing Topsoe's strategic considerations for a stepping stone approach to reach future markets.*

**Bridging the gap - First commercial contracts for eCOs™**

Based on the successful operation of the eCOs™ demonstration unit, followed by persistent, dedicated, and hard work by several groups at Haldor Topsoe, the company has recently signed the first commercial contract for ***two*** larger eCOs™ units[4]. The units will be able to produce up to 96 $Nm^3/h$ CO each with ultra-high purity. These contracts are a confirmation that the electrolysis technology can solve current challenges in the industry at a cost-competitive price, once appropriate niche markets are targeted. Furthermore, the increased interest and belief in the SOEC technology will certainly be strengthened by these contracts and is hopefully the first step in bridging the gap towards more sales and introduction of SOEC and eCOs™ on larger markets in the coming years.

### *1.5.7 Dissemination activities*

The following dissemination activities have been performed during the project

**Peer-reviewed publications**


1. Molla T. T., Kwok K., Frandsen H. L., Efficient modeling of metallic interconnects for thermo-mechanical simulation of SOFC stacks: homogenized behaviors and effect of contact, International Journal of Hydrogen Energy 41, 6433-6444 (2016).
2. Duhn, J. D., Jensen, A. D., Wedel, S., Wix, C., Modeling of Gas Diffusion in Ni/YSZ Electrodes in CO2 and co-electrolysis, Fuel Cells 17, 442-456 (2017).
3. Mogensen M.B., Ebbesen S.D., Jensen S.H., Sun X., Hauch A., Chen M. Concentration impedance in testing of solid oxide cells revisited, ECS Transactions 78, 2133-2139 (2017).
4. Hansen K.V., Norrman K., Traulsen M.L., Mogensen M.B., Dynamic and Impure Perovskite Structured Metal Oxide Surfaces, ECS Transactions 80, 91-100 (2017).
5. Kiebach R., Agersted K., Zielke P., Ritucci I., Brock M.B., Hendriksen P.V., A Novel SOFC/SOEC Sealing Glass with a Low SiO2 Content and a High Thermal Expansion Coefficient, ECS Transactions 78, 1739-1747 (2017).
6. Küngas R., Blennow P., Heiredal-Clausen T., Holt T., Rass-Hansen J., Primdahl S., Systematic Lifetime Testing of Stacks in CO2 Electrolysis, ECS Transactions 78, 2895-2905 (2017).
7. Jensen S. H., Langnickel H., Hintzen N., Chen M., Sun X., Hauch A., Butera G., Clausen, L. R., Reversible Operation of a Pressurized Solid Oxide Cell Stack Using Carbonaceous Gases, Journal of Energy Storage 22, 106-115 (2019).
8. Molla T. T., Kwok K., Frandsen H. L., Modelling the mechanical integrity of generic solid oxide cell stack designs exposed to long-term operation, Fuel Cells 19, 96-109 (2019).
9. Butera G., Jensen S. H., Clausen L. R., A novel system for large-scale storage of electricity as syntheticnatural gas using reversible pressurized solid oxide cells, Energy 166, 738-754 (2019).
10. Clausen L. R., Butera G., Jensen S. H., High efficiency SNG production from biomass and electricity by integrating gasification with pressurized solid oxide electrolysis cells, Energy 172, 1117-1131 (2019).


[4] https://blog.topsoe.com/delille-oxygen-co.-leases-two-ecos-units-for-cost-competitive-onsite-co-production

11. Küngas R., Blennow P., Heiredal-Clausen T., Nørby T.H., Rass-Hansen J., Moses P.G., Lifetime capacity – an important performance metric for SOEC stacks, *submitted for* ECS Transactions (SOFC-XVI), 2019.
12. Küngas R., Blennow P., Heiredal-Clausen T., Nørby T.H., Rass-Hansen J., Hansen J.B., Moses P.G., Progress in SOEC development activities at Haldor Topsoe, *submitted for* ECS Transactions (SOFC-XVI), 2019.

**Conference proceedings**

1. Blennow P., Rass-Hansen J., Heiredal-Clausen T., Küngas R., Nørby T.H., Primdahl S., Understanding lifetime limitations in the Topsoe Stack Platform using modeling and post mortem analysis, 12th European SOFC & SOEC Forum, Lucerne, Switzerland, (2016).
2. Jensen S. H., Langnickel H., Hintzen N., Chen M., Sun X., Hauch A., Butera G., Clausen, L. R., Pressurized reversible operation of a 30-cell solid oxide cell stack using carbonaceous gases. In V. Cigolotti (Ed.), Proceedings of the 7th European Fuel Cell Technology & Applications Conference (EFC2017), 413-414 (2017).
3. Hauch A., Skafte T. L., Küngas R., Traulsen M. L., and Jensen S. H., CO2 electrolysis – how gas purity and over-potential affect detrimental carbon deposition, 13th European SOFC & SOE Forum, Lucerne, Switzerland, B1501 (2018).
4. Jensen S.H., Hauch A., Sun X., Chen M., Ebbesen S.D., Mogensen M., Diffusion rates of reactants and components in solid oxide cells, 13th European SOFC & SOE Forum, Lucerne, Switzerland, B1208 (2018).
5. Küngas R., Blennow P., Heiredal-Clausen T., Nørby T. H., Rass-Hansen J., Moses P. G., Increasing the lifetime of stacks in CO2 electrolysis, 13th European SOFC & SOE Forum, Lucerne, Switzerland, B1503 (2018).
6. Nørby T. H., Küngas R., Blennow P., Heiredal-Clausen T., Rass-Hansen J., Moses P. G., High temperature measurement of air-side interconnect coating solutions, 13th European SOFC & SOE Forum, Lucerne, Switzerland, B1308 (2018).
7. Küngas R., Blennow P., Heiredal-Clausen T., Nørby T. H., Rass-Hansen J., Hansen J. B., Moses P. G., SOEC activities at Haldor Topsoe: status and perspectives on electrification of the chemical industry, 13th European SOFC & SOE Forum, Lucerne, Switzerland, A0501 (2018).

**Conference presentations**

1. Blennow P., Understanding lifetime limitations in the Topsoe Stack Platform using modeling and post mortem analysis, 12th European SOFC & SOEC Forum, 5-8 July 2016, Lucerne, Switzerland
2. Jensen S. H., Prime 2016, the 6th International ECS Electrochemical Energy Summit, October 2nd 2016, Hawaii Convention Center, Honolulu, USA.
3. Blennow P., CO from CO2 – on-site carbon monoxide on demand, invited talk, 1st International Conference on Electrolysis, 12-15 June 2017, Copenhagen, Denmark
4. Graves C., Skafte T.L., Carbon deposition in solid oxide electrochemical cells: Understanding, control, and prevention, invited talk, Solid State Ionics 21, 18 -23 June 2017, Padova, Italy.
5. Mogensen M., Ebbesen S.D., Jensen S.H., Sun X., Hauch A., Chen M., Concentration Impedance in Testing of Solid Oxide Cells Revisited, 15th International Symposium on Solid Oxide Fuel Cells, 23-28 July 2017, Hollywood, FL, USA.
6. Farandos N.M., Kelsall G.H., Rosa M., Gadea C., Skafte T.L., Kiebach R., Esposito V., Jensen S.H., Thin Inkjet Printed Tri-layer Electrolyte for Solid Oxide Cells, 2nd int. conf. on adv. energy mat. 11-13 September 2017, Surrey, England.
7. Hansen K.V, Norrman K., Traulsen M.L., Mogensen M., Dynamic and Impure Perovskite Structured Metal Oxide Surfaces, IMCC 11, 1-6/10 2017, Washington, DC, US.
8. Rass-Hansen J., Küngas R., Blennow P., Heiredal-Clausen T., Nørby T.H., Primdahl S. eCOs – a Commercial CO2 Electrolysis System Developed by Haldor Topsoe. 19th International Conference on Carbon Dioxide, 13-14/11 2017, Venice, Italy.
9. Blennow P. Perspectives with Electrolysis and Electrification for Making Sustainable Fuels and Chemicals, Sustain Conference 2017 at Technical University of Denmark, 6/12-2017, Denmark.
10. Jensen S. H., Langnickel H., Hintzen N., Chen M., Sun X., Hauch A., Butera G., Clausen L. R. Pressurized stack operation with carbonaceous gasses, Proc. of the 7th European Fuel Cell Technology & Applications Conference, 12-15 December 2017, Naples, Italy.

11. Jensen S. H., Langnickel H., Hintzen N., Chen M., Sun X., Hauch A., Butera G., Clausen L. R. Pressurized stack operation with carbonaceous gasses, Int. Adv. In applied Physics & Mat. Sci. Congress and Exhib. 24-30 April 2018, Oludeniz, Turkey.
12. Hauch A. High Temperature Electrolysis – Re-use of CO2 for synthetic fuels. 6th Int. Conf. on CO2 emission control and util. 15-17 June 2018, Hangzhou, China.
13. Jensen S.H., Hauch A., Sun X., Chen M., Ebbesen S.D., Mogensen M., Poster presentation: Diffusion rates of reactants and components in solid oxide cells, 13th European SOFC & SOE Forum 2018 Lucerne 3-6 July 2018. Switzerland.
14. Nørby T. H., Küngas R., Blennow P., Heiredal-Clausen T., Rass-Hansen J., Moses P. G. Poster presentation: High temperature measurement of air-side interconnect coating solutions, 13th European SOFC & SOE Forum, Lucerne 3-6 July 2018, Switzerland.
15. Küngas R., Blennow P., Heiredal-Clausen T., Nørby T. H., Rass-Hansen J., Moses P. G. Increasing the lifetime of stacks in CO2 electrolysis, 13th European SOFC & SOE Forum, 3-6 July 2018, Lucerne, Switzerland.
16. Küngas R., Blennow P., Heiredal-Clausen T., Nørby T. H., Rass-Hansen J., Hansen J. B., Moses P. G. SOEC activities at Haldor Topsoe: status and perspectives on electrification of the chemical industry, 13th European SOFC & SOE Forum, 3-6 July 2018, Lucerne, Switzerland.
17. Hauch A., Skafte T. L., Küngas R., Traulsen M. L., and Jensen S. H., CO2 electrolysis – how gas purity and over-potential affect detrimental carbon deposition, 13th European SOFC & SOE Forum, 3-6 July 2018, Lucerne, Switzerland.
18. P. Blennow, Power-to-X activities at HTAS: perspectives on electrification of the chemical industry, invited talk, Power2Gas Conference, 17-18 October 2018, Copenhagen, Denmark.
19. Hauch A., Chen M., Frandsen H. L., Hendriksen P. V., Khajavia P., Küngas R., Skafte T. L., Tong X., Trini M., Tripkovic D., Sun X. and Mogensen M. B., Solid Oxide Electrolysis Cells for Hydrogen and Synthetic Fuel Production from Renewable Energy, invited talk, MRS Spring meeting, 22-26/4 2019, Phoenix, AZ, USA
20. Blennow P., Power-to-X activities at Haldor Topsoe: a stepping-stone approach towards commercialization, invited talk, *to be presented* at 2nd International Conference on Electrolysis, 9-13/6-2019, Loen, Norway

**Other presentations and activities**

1. P. Blennow, trip to India to visit a number of companies for creating awareness of the eCOs technology (CO2 to CO using SOEC) – related to WP5 (CM2), October 2016, India.
2. Workshop at Foulum biogas plant together with EUDP project "El-upgraded Biogas" – related to WP5 (CM2), 31/10-1/11 - 2016, Foulum, Denmark.
3. P. Blennow, Poster presentation: Maturing SOEC, Den danske brint- og brændselscelledag, 10/11-2016, Odense, Denmark.
4. S. H. Jensen, IDA arr. 319899, Ingeniørforeningen i Danmark, February 21st 2017, Copenhagen, Denmark.
5. P. Blennow, Poster and presentation: Maturing SOEC, Den danske brint- og brændselscelledag, 28/11-2017, Odense, Denmark.
6. P. Blennow, Power-to-X, opportunities and challenges in a fossil-free future, invited talk, iGAS and IDA Kemi thematic meeting on "Emmisioner fra fremtidens energikilder", 7/6-2018, Copenhagen, Denmark.
7. P. Blennow, Power-to-X, opportunities and challenges in a fossil-free future, invited talk, Joint Workshop on Route to the Industrialisation of High-Temperature Electrolysis, 3/9-2018, Salzgitter, Germany
8. P. Blennow, Invited speaker at CPH Climate Solutions, Workshop on Carbon Capture and Usage, Copenhagen, 12/11-2018
9. P. Blennow, Poster: Maturing SOEC, Den danske brint- og brændselscelledag, 19/11-2018, Odense, Denmark.
10. P. Blennow, Power-to-X activities at HTAS: perspectives on electrification of the chemicals industry, Invited talk, DTU Energy Symposium 2018, 13/12-2018, Roskilde, Denmark

## 1.6 Utilization of project results

For Danish Solar Energy (DSOL) the project has showed big potential of using hydrogen as a future potential future energy storage form. They have developed all needed interfaces to integrate electrolysis with solar energy, but there are still challenges maturing the SOEC/SOFC for this specific purpose, mainly related to cost. Alternative electrolysis technologies such as alkaline electrolysis (AEC) and/or proton exchange membrane electrolysis cell (PEMEC) could be intermediate alternatives.

The knowledge DSOL has gained through this project, hereby the developed power electronics (SMART controller), will be used in their other solar energy storage solutions, e.g. battery storage solutions. With the gained knowledge from this project, DSOL are now able to predict several key factors to optimize the storage solutions, which will give them an advantage to supply custom-made solutions and hereby optimize and reduce the system cost and extend their sale.

For Haldor Topsoe it is more than fair to say that the Maturing SOEC project has facilitated improved confidence in the SOEC technology, both internally at Topsoe and externally. The improved TSP-1 stacks developed during the project, having a projected lifetime >2 years, will be used in coming SOEC projects and in commercial offerings to end-customers. Based on the results achieved in the project, Topsoe has submitted three patent applications related to improvement of specific stack components.

The improved modelling tools developed in the project will be used for future stack modifications and to conduct virtual prototyping, which will save development time and speed up the time from idea to product. The primary focus the coming 1-3 years is to fully commercialize the eCOs™ technology in various niche markets and increase the awareness and potential with the technology. Topsoe has a strong IP portfolio related to eCOs™, which gives them an advantage in further maturing the SOEC technology, where their already cost-competitive eCOs™ technology can be used with a stepping-stone approach, to reach future larger markets for electrification of the chemicals industry and Power-to-X.

DTU has obtained novel insights of technologically relevant degradation issues during the Maturing SOEC project. Long-term testing on single-cell level has furthered knowledge of Ni migration, contact issues between cell and interconnect, requirement of gas purity, and carbon deposition. Studies of these mechanisms have continued in projects running alongside the Maturing SOEC project, and several are continuing in new projects. Likewise, one of the cell design strategies developed during the project will be pursued in new projects and a patent application case is under consideration.

Furthermore, the learnings from stack testing in the project have put DTU in a strong position as one of the world-leading institutions capable of advanced SOEC-stack testing. Especially the improvement of impedance measurements and analysis on large commercial stacks, and the experience gained from this, is vital for future project applications. The equipment and vast amount of knowledge build up during the trials with pressurized testing puts DTU in a league of its own when it comes to complex stack testing.

## 1.7 Project conclusion and perspective

At the core of Haldor Topsoe's electrolysis approach lies the Topsoe Stack Platform (TSP-1), a stack technology based on solid oxide cells that can run in both electrolysis and fuel cell mode. The development of the TSP-1 has had a strong focus on stack robustness, which means delivering a reliable and manufacturable stack design that can handle typical situations from real-life operation at customer sites. The current generation of SOC stacks, the TSP-1, was originally developed for SOFC (fuel cell) operation in Topsoe Fuel Cell (TOFC). Since the closure of TOFC in 2014, the TSP-1 stack has been improved, where a number of stack components have been modified, and now works very well in both fuel cell and electrolysis mode.

In this project, significant progress was made on improving degradation and robustness both on cell and stack level. Furthermore, improved multi-physics modelling tools were developed for faster evaluation of design modifications. The simulation tools were also successfully used for finding safe operating protocols for various electrolysis modes.

More than one year operation in $CO_2$ electrolysis was shown in a system level test (SOEC Core), and improved stacks at the end of the project showed potential for lifetimes >2 years (tests still ongoing). Many of the learnings from this project have or will be implemented in coming upgrades to Topsoe's TSP-1 stack. The results will hopefully facilitate market penetration in certain niche markets for SOEC. HTAS is currently focusing on commercialization of their unique cost-competitive eCOs™ technology for converting $CO_2$ to CO, which is relevant for several different industries.

In the longer perspective, the TSP-1 stack design has some design limitations that inhibits its full capacity in electrolysis mode. Topsoe will therefore aim to develop a new version, the TSP-2. The new stack platform will be designed purely for electrolysis operation, meaning that it should be able to perform both steam electrolysis (for $H_2$ production) and $CO_2$ electrolysis (for CO production) with high efficiency. Topsoe will focus on maintaining the high robustness features of TSP-1 and aim for substantially increasing stack lifetime and lower stack production costs. The learnings from Maturing SOEC (improvement of stack components, furthered understanding of lifetime limitations, improved modelling tools etc) will be passed on to the next stack platform. In order to achieve the goals for the new stack and systems, as well as finding new markets using the stepping-stone approach described above, collaboration and investments are essential. Topsoe has therefore applied (and will apply) for a number of different projects during 2018/2019, and onwards, to support these development efforts.

## Annex

### *References in WP1 (section 1.5.2):*


[1] P.H. Larsen, K. Brodersen, Reversible solid oxide cell producing method involves sintering multilayer structure after laminating anode support layer on top of anode layer, US2008124602-A1; JP2008130568-A; EP1930974-A1; CN101242003-A; CA2611362-A1; KR2008047282-A; KR966845-B1, 2008.

[2] J. Hjelm, M. Soegaard, R. Knibbe, A. Hagen, M. Mogensen, Electrochemical Characterization of Planar Anode Supported SOFC with Strontium-Doped Lanthanum Cobalt Oxide Cathodes, in: ECS Trans., ECS, 2008: pp. 285–299. doi:10.1149/1.3050400.

[3] A. Hauch, C. Birkl, K. Brodersen, P.S. Jørgensen, Multilayer tape cast SOFC - Effect of sintering temperature, Proc. - 10th Eur. Solid Oxide Fuel Cell Forum. Chapter 8 (2012) 62–71.

[4] S.H. Jensen, A. Hauch, P.V. Hendriksen, M. Mogensen, Advanced Test Method of Solid Oxide Cells in a Plug-Flow Setup, J. Electrochem. Soc. 156 (2009) B757. doi:10.1149/1.3116247.

[5] S.D. Ebbesen, C. Graves, A. Hauch, S.H. Jensen, M. Mogensen, Poisoning of Solid Oxide Electrolysis Cells by Impurities, J. Electrochem. Soc. 157 (2010) B1419. doi:10.1149/1.3464804.

[6] M.B. Mogensen, A. Hauch, X. Sun, M. Chen, Y. Tao, S.D. Ebbesen, K. V Hansen, P. V Hendriksen, Relation Between Ni Particle Shape Change and Ni Migration in Ni-YSZ Electrodes - a Hypothesis, Fuel Cells. 17 (2017) 434–441. doi:10.1002/fuce.201600222.

[7] A. Hauch, K. Brodersen, M. Chen, M.B. Mogensen, Ni/YSZ electrodes structures optimized for increased electrolysis performance and durability, Solid State Ionics. 293 (2016) 27–36. doi:10.1016/j.ssi.2016.06.003.

[8] S.D. Ebbesen, M. Mogensen, Exceptional Durability of Solid Oxide Cells, Electrochem. Solid-State Lett. 13 (2010) B106. doi:10.1149/1.3455882.

[9] T.L. Skafte, C. Graves, P. Blennow, J. Hjelm, Carbon deposition and sulfur poisoning during CO2 electrolysis in Ni-based solid-oxide-cell electrodes, Submitted. (2017).

[10] K. Brodersen, A. Hauch, M. Chen, J. Hjelm, Durable Fuel Electrode, Patent WO2017029350, 2017.

[11] A. Hauch, F. Karas, K. Brodersen, M. Chen, No Title, in: Proc. 11th Eur. SOFC SOE Forum, 2014: p. 88.

[12] M. Chen, Y.-L. Liu, J.J. Bentzen, W. Zhang, X. Sun, a. Hauch, Y. Tao, J.R. Bowen, P. V. Hendriksen, Microstructural Degradation of Ni/YSZ Electrodes in Solid Oxide Electrolysis Cells under High Current, J. Electrochem. Soc. 160 (2013) F883–F891. doi:10.1149/2.098308jes.

[13] M.A. Pimenta, G. Dresselhaus, M.S. Dresselhaus, L.G. Cançado, A. Jorio, R. Saito, Studying disorder in graphite-based systems by Raman spectroscopy, Phys. Chem. Chem. Phys. 9 (2007) 1276–1290. doi:10.1039/B613962K.

[14] V. Duboviks, R.C. Maher, M. Kishimoto, L.F. Cohen, N.P. Brandon, G.J. Offer, A Raman spectroscopic study of the carbon deposition mechanism on Ni/CGO electrodes during CO/CO2 electrolysis, Phys. Chem. Chem. Phys. 16 (2014) 13063. doi:10.1039/c4cp01503g.

[15] J.F.B. Rasmussen, A. Hagen, The effect of H2S on the performance of Ni-YSZ anodes in solid oxide fuel cells, J. Power Sources. 191 (2009) 534–541. doi:10.1016/j.jpowsour.2009.02.001.

[16] A. Hauch, A. Hagen, J. Hjelm, T. Ramos, Sulfur Poisoning of SOFC Anodes: Effect of Overpotential on Long-Term Degradation, J. Electrochem. Soc. 161 (2014) F734–F743. doi:10.1149/2.080406jes.

[17] H. Kishimoto, A. Suzuki, T. Shimonosono, Agglomeration behavior of nickel particles on YSZ electrolyte, Solid State Ionics. 225 (2012) 65–68. doi:10.1016/j.ssi.2012.04.010.

[18] C.H. Law, S.W. Sofie, Anchoring of Infiltrated Nickel Electro-Catalyst by Addition of Aluminum Titanate, J. Electrochem. Soc. 158 (2011) B1137. doi:10.1149/1.3610226.


### *References in WP2 (section 1.5.3):*


[1] R.R. Mosbaek, J. Hjelm, R. Barfod, J. Høgh, P. V. Hendriksen, Electrochemical Characterization and Degradation Analysis of Large SOFC Stacks by Impedance Spectroscopy, Fuel Cells. 13 (2013) 605–611. doi:10.1002/fuce.201200175.

[2] R.R. Mosbæk, Solid Oxide Fuel Cell Stack Diagnostics, 2014.

[3] C. Graves, Reversing and Repairing Microstructure Degradation in Solid Oxide Cells during Operation, ECS Trans. 57 (2013) 3127–3136. doi:10.1149/05701.3127ecst.

[4] T.L. Skafte, Lifetime limiting effects in pre-commercial solid oxide cell devices, 2017.

[5] X. Sun, M. Chen, S.H. Jensen, S.D. Ebbesen, C. Graves, M. Mogensen, Thermodynamic analysis of synthetic hydrocarbon fuel production in pressurized solid oxide electrolysis cells, Int. J. Hydrogen Energy. 37 (2012) 17101–17110. doi:10.1016/j.ijhydene.2012.08.125.

[6] J.-C. Njodzefon, C.R. Graves, M.B. Mogensen, A. Weber, J. Hjelm, Kinetic Studies on State of the Art Solid Oxide Cells: A Comparison between Hydrogen/Steam and Reformate Fuels, J. Electrochem. Soc. 163 (2016) F1451–F1462. doi:10.1149/2.1201613jes.

[7] M. Chen, X. Sun, C. Chatzichristodoulou, S. Koch, P.V. Hendriksen, M.B. Mogensen, Thermoneutral Operation of Solid Oxide Electrolysis Cells in Potentiostatic Mode, ECS Trans. 78 (2017) 3077–3088. doi:10.1149/07801.3077ecst.
[8] M.B. Mogensen, A. Hauch, X. Sun, M. Chen, Y. Tao, S.D. Ebbesen, K. V Hansen, P. V Hendriksen, Relation Between Ni Particle Shape Change and Ni Migration in Ni-YSZ Electrodes - a Hypothesis, Fuel Cells. 17 (2017) 434–441. doi:10.1002/fuce.201600222.
[9] Y. Tao, S.D. Ebbesen, M.B. Mogensen, Degradation of solid oxide cells during co-electrolysis of steam and carbon dioxide at high current densities, J. Power Sources. 328 (2016) 452–462. doi:10.1016/j.jpowsour.2016.08.055.
[10] T.L. Skafte, P. Blennow, J. Hjelm, C. Graves, Carbon deposition and sulfur poisoning during CO2 electrolysis in nickel-based solid oxide cell electrodes, J. Power Sources. 373 (2018) 54–60. doi:10.1016/j.jpowsour.2017.10.097.
[11] Y. Tao, S.D. Ebbesen, M.B. Mogensen, Carbon Deposition in Solid Oxide Cells during Co-Electrolysis of H2O and CO2, J. Electrochem. Soc. 161 (2014) F337–F343. doi:10.1149/2.079403jes.
[12] Y. Tao, S.D. Ebbesen, W. Zhang, M.B. Mogensen, Carbon Nanotube Growth on Nanozirconia under Strong Cathodic Polarization in Steam and Carbon Dioxide, ChemCatChem. 4000 (2014) 1220–1224. doi:10.1002/cctc.201300941.
[13] S. McIntosh, J.M. Vohs, R.J. Gorte, Role of Hydrocarbon Deposits in the Enhanced Performance of Direct-Oxidation SOFCs, J. Electrochem. Soc. 150 (2003) A470. doi:10.1149/1.1559064.
[14] H. He, R.J. Gorte, J.M. Vohs, Highly Sulfur Tolerant Cu-Ceria Anodes for SOFCs, Electrochem. Solid-State Lett. 8 (2005) A279. doi:10.1149/1.1896469.
[15] T. Matsui, K. Eguchi, K. Shirai, T. Okanishi, H. Muroyama, K. Eguchi, New Design Concept of Ni–Doped-Ceria Cermet Anode for Solid Oxide Fuel Cells: Redox-Induced Self-Modification, ECS Trans. 78 (2017) 1115–1123. doi:10.1149/07801.1115ecst.
[16] R. Knibbe, M.L. Traulsen, A. Hauch, S.D. Ebbesen, M. Mogensen, Solid Oxide Electrolysis Cells: Degradation at High Current Densities, J. Electrochem. Soc. 157 (2010) B1209. doi:10.1149/1.3447752.
[17] G. Rinaldi, S. Diethelm, E. Oveisi, P. Burdet, J. Van herle, D. Montinaro, Q. Fu, A. Brisse, Post-test Analysis on a Solid Oxide Cell Stack Operated for 10,700 Hours in Steam Electrolysis Mode, Fuel Cells. (2017) 1–9. doi:10.1002/fuce.201600194.

***References in WP3 (section 1.5.4):***

[1] T.T. Molla, K. Kwok, H.L. Frandsen, Efficient modeling of metallic interconnects for thermo-mechanical simulation of SOFC stacks: Homogenized behaviors and effect of contact, Int. J. Hydrogen Energy. 41 (2016) 6433-6444. doi: 10.1016/j.ijhydene.2016.03.002.
[2] J.D. Duhn, A.D. Jensen, S. Wedel, C. Wix, Modeling of Gas Diffusion in Ni/YSZ Electrodes in CO2 and Co-electrolysis, Fuel Cells. 17 (2017) 442-456. doi: 10.1002/fuce.201700068
[3] H.L. Frandsen, M. Navasa, T.T. Molla, P.V. Hendriksen, Computational efficient 3D multiphysics models to estimate the long-term mechanical behavior of SOC stacks, Proceedings of 13th European SOFC & SOE Forum 2018, A1402 (2018).

***References in WP4 (section 1.5.5):***

[1] C. Graves, S.D. Ebbesen, S.H. Jensen, S.B. Simonsen, M.B. Mogensen, Eliminating degradation in solid oxide electrochemical cells by reversible operation, Nat. Mater. 14 (2015) 239–244. doi:10.1038/nmat4165.